



# Estimates of Lightning $\text{NO}_x$ Production based on High Resolution OMI $\text{NO}_2$ Retrievals over the Continental US

Xin Zhang<sup>1,2</sup>, Yan Yin<sup>1,2</sup>, Ronald van der A<sup>2,3</sup>, Jeff L. Lapierre<sup>4</sup>, Qian Chen<sup>1,2</sup>, Xiang Kuang<sup>1,2</sup>,  
Shuqi Yan<sup>2</sup>, Jinghua Chen<sup>1,2</sup>, Chuan He<sup>1,2</sup>, and Rulin Shi<sup>1,2</sup>

<sup>1</sup> Collaborative Innovation Center on Forecast and Evaluation of Meteorological Disasters/Key Laboratory for Aerosol-Cloud-Precipitation of China Meteorological Administration, Nanjing University of Information Science and Technology (NUIST), Nanjing 210044, China

<sup>2</sup> Department of Atmospheric Physics, Nanjing University of Information Science and Technology (NUIST), Nanjing 210044, China

<sup>3</sup> Royal Netherlands Meteorological Institute (KNMI), Department of Satellite Observations, De Bilt, the Netherlands

<sup>4</sup> Earth Networks, Germantown, Maryland, USA

**Correspondence:** Yan Yin (yinyan@nuist.edu.cn)

**Abstract.** Lightning serves as the dominant source of nitrogen oxides ( $\text{NO}_x = \text{NO} + \text{NO}_2$ ) in the upper troposphere (UT), with strong impact on ozone chemistry and the hydroxyl radical production. However, the production efficiency (PE) of lightning nitrogen oxides ( $\text{LNO}_x$ ) is still quite uncertain (32 – 1100 mol NO per flash). Satellites measurements are a powerful tool to estimate  $\text{LNO}_x$  directly as compared to conventional platforms. To apply satellite data in both clean and polluted regions, a new algorithm for calculating  $\text{LNO}_x$  has been developed based on the program of new Berkeley High Resolution (BEHR) v3.0B  $\text{NO}_2$  product and the Weather Research and Forecasting-Chemistry (WRF-Chem) model.  $\text{LNO}_x$  PE over the continental US is estimated using the  $\text{NO}_2$  product of the Ozone Monitoring Instrument (OMI) satellite and the Earth Networks Total Lightning Network (ENTLN) data. Focusing on the summer season during 2014, we find that the lightning  $\text{NO}_2$  ( $\text{LNO}_2$ ) PE is  $44 \pm 16$  mol  $\text{NO}_2$  flash<sup>-1</sup> and  $8 \pm 3$  mol  $\text{NO}_2$  stroke<sup>-1</sup> while  $\text{LNO}_x$  PE is  $120 \pm 52$  mol  $\text{NO}_x$  flash<sup>-1</sup> and  $22 \pm 9$  mol  $\text{NO}_x$  stroke<sup>-1</sup>. Results reveal that former methods are more sensitive to background  $\text{NO}_2$  and neglect much of the below-cloud  $\text{LNO}_2$ . As the  $\text{LNO}_x$  parameterization varies in studies, the sensitivity of our calculations to the setting of the amount of lightning NO (LNO) is evaluated. Careful consideration of the ratio of  $\text{LNO}_2$  to  $\text{NO}_2$  is also needed, given its large influence on the estimation of  $\text{LNO}_2$  PE.

## 1 Introduction

Nitrogen oxides ( $\text{NO}_x$ ) near the Earth's surface is mainly produced by soil, biomass burning and fossil fuel combustion, while  $\text{NO}_x$  in the middle and upper troposphere originate largely from lightning and aircraft emissions.  $\text{NO}_x$  plays an important role in the production of ozone ( $\text{O}_3$ ) and the hydroxyl radical (OH). While the anthropogenic sources of  $\text{NO}_x$  are largely known, lightning nitrogen oxides ( $\text{LNO}_x$ ) are still the source with the greatest uncertainty, though they are estimated to range between 2 and 8 Tg N yr<sup>-1</sup> (Schumann and Huntrieser, 2007).  $\text{LNO}_x$  is produced in the upper troposphere (UT) by  $\text{O}_2$  and  $\text{N}_2$  dissociation in the hot lightning channel as described by the Zel'dovich mechanism (Zel'dovich and Raizer, 1967). With the recent updates



of UT NO<sub>x</sub> chemistry, the day time lifetime of UT NO<sub>x</sub> is evaluated to be ~ 3 h near thunderstorms and ~ 0.5 – 1.5 days away from thunderstorms (Nault et al., 2016, 2017). This results in enhanced O<sub>3</sub> production in the cloud outflow of active convection (Pickering et al., 1996; Hauglustaine et al., 2001; DeCaria et al., 2005; Ott et al., 2007; Dobber et al., 2008; Allen et al., 2010; Finney et al., 2016). As O<sub>3</sub> is known as a greenhouse gas, strong oxidant and absorber of ultraviolet radiation (Myhre et al., 2013), the contributions of LNO<sub>x</sub> to O<sub>3</sub> production also have an effect on climate forcing. Finney et al. (2018) found different impacts on atmospheric composition and radiative forcing when simulating future lightning using a new upward cloud ice flux (IFLUX) method and the commonly used the widely used cloud-top height (CTH) approach. As lightning with the CTH approach have reported 5 — 16% increases over the next century (Clark et al., 2017; Banerjee et al., 2014; Krause et al., 2014), a 15% decrease was estimated with IFLUX in 2100 under a strong global warming scenario (Finney et al., 2018). As a result of the different effects on compositions, a net positive radiative forcing was found with the CTH approach while there is little net radiative forcing with the IFLUX approach.

In the view of the region dependent lifetime of NO<sub>x</sub> and the difficulty of measuring LNO<sub>x</sub> directly, a better understanding of the LNO<sub>x</sub> production is required, especially in the tropical and mid-latitude regions in summer. Using its distinct spectral absorption lines in the near-ultraviolet (UV) and visible (VIS) range (Platt and Perner, 1983), NO<sub>2</sub> can be measured by satellite instruments like the Global Ozone Monitoring Experiment (GOME; Burrows et al., 1999; Richter et al., 2005), Scanning Imaging Absorption Spectrometer for Atmospheric Chartography (SCIAMACHY; Bovensmann et al., 1999), the Second Global Ozone Monitoring Experiment (GOME-2; Callies et al., 2000) and the Ozone Monitoring Instrument (OMI; Levelt et al., 2006). OMI has the highest spatial resolution, least instrument degradation and longest record among these satellites (Krotkov et al., 2017). Satellites measurements of NO<sub>2</sub> are a powerful tool compared to conventional platforms, because of its global coverage, constant instrument features and temporal continuity.

Recent studies have determined and qualified LNO<sub>x</sub> using satellite observations. Beirle et al. (2004) constrained the LNO<sub>x</sub> production to 2.8 (0.8 – 14) Tg N yr<sup>-1</sup> by combining GOME NO<sub>2</sub> data and flash counts from the Lightning Imaging Sensor (LIS) aboard the Tropical Rainfall Measurement Mission (TRMM) over Australia. Boersma et al. (2005) estimated the global LNO<sub>x</sub> production of 1.1 – 6.4 Tg N yr<sup>-1</sup> by comparing GOME NO<sub>2</sub> with distributions of LNO<sub>2</sub> modeled by Tracer Model 3 (TM3). Martin et al. (2007) analyzed SCIAMACHY NO<sub>2</sub> columns with Goddard Earth Observing System chemistry model (GEOS-Chem) simulations to identify LNO<sub>x</sub> production amounting to 6 ± 2 Tg N yr<sup>-1</sup>.

As these methods focus on monthly or yearly mean NO<sub>2</sub> column densities, more recent studies applied specific approaches to investigate LNO<sub>x</sub> directly over active convections. Beirle et al. (2006) estimated LNO<sub>x</sub> as 1.7 (0.6 – 4.7) Tg N yr<sup>-1</sup> based on a convective system over the Gulf of Mexico, using National Lightning Detection Network (NLDN) observations and GOME NO<sub>2</sub> column densities. However, it is assumed that all the enhanced NO<sub>2</sub> originated from lightning without the contribution of anthropogenic emissions. Beirle et al. (2010) analyzed LNO<sub>x</sub> production systematically using the global dataset of SCIAMACHY NO<sub>2</sub> observations combined with flash data from the World Wide Lightning Location Network (WWLLN). The threshold of high flash rates is that the summation of the corrected flashes within the satellite pixel (30 × 60 km<sup>2</sup>) in the last one hour must be greater than 1 flashes/km<sup>2</sup> /h. But the results of LNO<sub>x</sub> production are highly variable and correlations between flash rate densities and LNO<sub>x</sub> production are low in some cases. Bucseala et al. (2010) estimate LNO<sub>x</sub> production as ~ 100 –



250 mol NO<sub>x</sub>/flash for four cases, using the DC-8 and OMI data during NASA's Tropical Composition, Cloud and Climate Coupling Experiment (TC<sup>4</sup>).

Based on the approach used by Bucsele et al. (2010), a special algorithm was developed by Pickering et al. (2016) to retrieve LNO<sub>x</sub> from OMI and the WWLLN. The algorithm takes the OMI tropospheric slant column density (SCD) of NO<sub>2</sub> (S<sub>NO<sub>2</sub></sub>) as the tropospheric slant column density of LNO<sub>2</sub> (S<sub>LNO<sub>2</sub></sub>) by using cloud radiance fraction (CRF) greater than 0.9 to minimize or screen the lower tropospheric background. To convert the S<sub>LNO<sub>2</sub></sub> to the tropospheric vertical density (VCD) of LNO<sub>x</sub> (V<sub>LNO<sub>x</sub></sub>), an air mass factor (AMF) is calculated by dividing the a priori S<sub>LNO<sub>2</sub></sub> by the a priori V<sub>LNO<sub>x</sub></sub>. Since they assumed NO<sub>2</sub> above the cloud are all LNO<sub>2</sub>, their AMF and derived VCD of LNO<sub>x</sub> (LNO<sub>2</sub>) is named as AMF<sub>LNO<sub>x</sub>Clean</sub> and LNO<sub>x</sub>Clean (LNO<sub>2</sub>Clean), respectively. Unless otherwise specified, abbreviations S and V are respectively defined as the tropospheric SCD and VCD in this paper. The a priori S<sub>LNO<sub>2</sub></sub> is calculated using a radiative transfer model and a profile of LNO<sub>2</sub> simulated by the NASA Global Modeling Initiative (GMI) chemical transport model. The a priori V<sub>LNO<sub>x</sub></sub> is also obtained from the GMI model. Results for the Gulf of Mexico during 2007 – 2011 summer yield LNO<sub>x</sub> production of 80 ± 45 mol NO<sub>x</sub> per flash. Among several substantial sources of uncertainty, significant uncertainty (3% ~ >30%) exists in characterizing background NO<sub>x</sub> in this region (Pickering et al., 2016).

More recently Bucsele et al. (2019) obtained an average production efficiency (PE) of 180 ± 100 mol per flash over East Asia, Europe and North America based on the method used in Pickering et al. (2016). The tropospheric NO<sub>x</sub> background was removed by the weighted temporal average of NO<sub>x</sub> at each box which meets the optical cloud pressure and CRF criteria but has 0 — 1 flashes instead. The lofted pollution was corrected by 15% according to the estimation from DeCaria et al. (2000, 2005) and the average chemical delay was adjusted by 15% following the 3-hour LNO<sub>x</sub> lifetime in the nearby field of convection (Nault et al., 2017). However, there were negative LNO<sub>x</sub> values caused by the overestimation of the tropospheric background at those locations.

On another hand, Lapierre et al. (2019) constrained LNO<sub>2</sub> to 1.1 ± 0.6 mol NO<sub>2</sub>/stroke for intracloud (IC) strokes and 10.0 ± 4.9 mol NO<sub>2</sub>/stroke for cloud-to-ground (CG) strokes over the continental US (CONUS). LNO<sub>2</sub> per stroke was scaled to 54.4 mol NO<sub>x</sub>/flash by strokes per flash and the ratio of NO to NO<sub>2</sub> in the UT. They used the regridded Berkeley High-Resolution (BEHR) V3.0A 0.05° × 0.05° "visible only" NO<sub>2</sub> VCD (V<sub>vis</sub>) product which includes two parts of NO<sub>2</sub> can be "seen" by the satellite. The first part is the NO<sub>2</sub> above clouds and the second part is the NO<sub>2</sub> detected from cloud free areas. A threshold of 3 × 10<sup>15</sup> molecules cm<sup>-2</sup>, the typical urban NO<sub>2</sub> concentration, was applied to mask the contaminated grid cells (Beirle et al., 2010; Laughner and Cohen, 2017). The main difference between Lapierre et al. (2019) and Pickering et al. (2016) is the air mass factor for lightning (AMF<sub>LNO<sub>x</sub></sub>) implemented in the basic algorithm. In Lapierre et al. (2019), the air mass factor was used to convert S<sub>NO<sub>2</sub></sub> to V<sub>vis</sub>, while in Pickering et al. (2016) it was used to convert S<sub>LNO<sub>2</sub></sub> to V<sub>LNO<sub>x</sub></sub>, assuming that all S<sub>NO<sub>2</sub></sub> is generated by lightning.

To apply the approach used by Bucsele et al. (2010), Pickering et al. (2016), Bucsele et al. (2019) and Lapierre et al. (2019) without geographic restrictions, contamination of anthropogenic emissions must be taken into account in detail. The Weather Research and Forecasting (WRF) model coupled with chemistry (WRF-Chem) has been employed to evaluate the convective transport and chemistry in many studies (Barth et al., 2012; Wong et al., 2013; Fried et al., 2016; Li et al., 2017). Meanwhile,



Laughner and Cohen (2017) showed that the OMI AMF is increased by  $\sim 35\%$  for summertime when  $\text{LNO}_2$  simulated by WRF-Chem is included in the a priori profiles to match aircraft observations. The simulation agrees with observed  $\text{NO}_2$  profiles and the bias of AMF is reduced to  $< \pm 4\%$  for OMI viewing geometries.

In this paper, we focused on the estimation of  $\text{LNO}_2$  production per flash ( $\text{LNO}_2/\text{flash}$ ),  $\text{LNO}_x$  production per flash ( $\text{LNO}_x/\text{flash}$ ),  
95  $\text{LNO}_2$  production per stroke ( $\text{LNO}_2/\text{stroke}$ ) and  $\text{LNO}_x$  production per stroke ( $\text{LNO}_x/\text{stroke}$ ) in May–August (MJJA) 2014 by  
developing an algorithm similar to Pickering et al. (2016) based on the BEHR  $\text{NO}_2$  retrieval algorithm (Laughner et al., 2018a,  
b), but it performs better over background  $\text{NO}_2$  sources. Section 2 describes the satellite, lightning data, model settings and the  
algorithm in detail. Section 3 explores the suitable data criteria, compares different methods and evaluates the effect of cloud  
and  $\text{LNO}_x$  parameterization on  $\text{LNO}_x$  production estimation. Section 4 examines different sources of the uncertainty of the  
100 results. Conclusions are summarized in Section 5.

## 2 Data and Methods

### 2.1 Ozone Monitoring Instrument (OMI)

OMI is carried on the Aura satellite (launched in 2004), a member of A-train satellite group (Levelt et al., 2006, 2018). OMI  
passes over the equator at  $\sim 13:45$  LT (ascending node) and has a swath width of 2600 km, with a nadir field-of-view resolution  
105 of  $13 \times 24 \text{ km}^2$ . Since the beginning of 2007, some of the measurements have become useless as a result of anomalous radiances  
called the “row anomaly” (Dobber et al., 2008). For the current study, we used the NASA standard product v3 (Krotkov et al.,  
2017) as input to the  $\text{LNO}_x$  retrieval algorithm.

The main steps of calculating the  $\text{NO}_2$  tropospheric VCD ( $V_{\text{NO}_2}$ ) in the NASA product include:

1. SCDs are determined by the OMI-optimized differential optical absorption spectroscopy (DOAS) spectral fit;
- 110 2. A corrected (“de-striped”) SCD is obtained by subtracting the bias from the measured slant column;
3. The AMF for stratospheric ( $\text{AMF}_{\text{strat}}$ ) or tropospheric column ( $\text{AMF}_{\text{trop}}$ ) is calculated from the  $\text{NO}_2$  profile integrated  
vertically using weighted scattering weights with the a priori profiles. These profiles are obtained from GMI monthly mean  
profiles using four years (2004 – 2007) simulation;
4. The stratospheric  $\text{NO}_2$  VCD ( $V_{\text{strat}}$ ) is calculated from the subtraction of a priori contribution from tropospheric  $\text{NO}_2$  and  
115 a three-step (interpolation, filtering, and smoothing) algorithm (Bucsela et al., 2013);
5.  $V_{\text{strat}}$  is converted to the slant column using  $\text{AMF}_{\text{strat}}$  and subtracted from the measured SCDs to yield  $S_{\text{NO}_2}$ , leading to  
 $V_{\text{NO}_2} = S_{\text{NO}_2}/\text{AMF}_{\text{trop}}$ .

Based on this method, we developed a new  $\text{AMF}_{\text{LNO}_x}$  to obtain the desired  $V_{\text{LNO}_x}$  ( $V_{\text{LNO}_x} = S_{\text{NO}_2}/\text{AMF}_{\text{LNO}_x}$ ) to replace the  
original step 5. Details of this algorithm are discussed in section 2.4.



## 120 2.2 The Earth Networks Total Lightning Detection Network (ENTLN)

The Earth Networks Total Lightning Network (ENTLN) operates a system of over 1500 ground-based stations around the world with more than 900 sensors installed in the CONUS (Zhu et al., 2017). Both IC and CG lightning flashes are located by the sensors with detection frequency ranging from 1 Hz to 12 MHz based on the electric field pulse polarity and wave shapes. Groups of pulses are classified as a flash if they are within 700 ms and 10 km. In the preprocessed data obtained from the  
125 ENTLN, both strokes and lightning flashes composed of one or more strokes are included.

Rudlosky (2015) compared ENTLN with LIS and found that the relative flash detection efficiency of ENTLN increases from 21.6% during 2011 to 31.4% during 2013. Lapierre et al. (2019) also compared combined ENTLN and the NLDN dataset with data from the LIS and the detection efficiencies of IC flashes and strokes are 88% and 45%, respectively. Since we use the ENTLN data in 2014 as Lapierre et al. (2019) and NLDN detection efficiency of IC pulses should be lower than 33% which is  
130 calculated by the data in 2016 (Zhu et al., 2016), only the IC flashes and strokes are corrected by 88% and 45%, respectively, while CG flashes and strokes are unchanged because of the high detection efficiency.

## 2.3 Model Description

The present study uses WRF-Chem version 3.5.1 (Grell et al., 2005) with a horizontal grid size of  $12 \times 12$  km and 29 vertical levels (Fig. 1). The initial and boundary conditions of meteorological parameters are provided by the North American  
135 Regional Reanalysis (NARR) dataset with a 3 hourly time resolution. Based on Laughner et al. (2018b), 3D wind fields, temperature and water vapor are nudged towards the NARR data. Outputs from the version 4 of Model for Ozone and Related chemical Tracers (MOZART-4; Emmons et al., 2010) was used to generate the initial and boundary conditions of chemical species. Anthropogenic emissions are driven by the 2011 National Emissions Inventory (NEI), scaled to model years by the Environmental Protection Agency annual total emissions (EPA and OAR, 2015). The Model of Emissions of Gases and Aerosol  
140 from Nature (MEGAN; Guenther et al., 2006) is used for biogenic emissions. The chemical mechanism is the version 2 of Regional Atmospheric Chemistry Mechanism (RACM2; Goliff et al., 2013) with updates from Browne et al. (2014) and Schwantes et al. (2015). In addition, lightning flash rate and  $\text{LNO}_x$  parameterizations are activated ( $200 \text{ mol NO flash}^{-1}$ , the factor to adjust the predicted number of flashes is set to 1; hereinafter referred to as " $1 \times 200 \text{ mol NO flash}^{-1}$ "). The bimodal profile modified from the standard Ott et al. (2010) profile (Laughner and Cohen, 2017) is employed as the vertical distribution  
145 of lightning NO (LNO) in WRF-Chem, while LNO and  $\text{LNO}_2$  profiles are defined as the difference of vertical profiles between simulations with and without lightning.

## 2.4 Method for Deriving AMF

The  $V_{\text{LNO}_x}$  near convection is calculated according:

$$V_{\text{LNO}_x} = \frac{S_{\text{NO}_2}}{\text{AMF}_{\text{LNO}_x}} \quad (1)$$



150 where  $S_{\text{NO}_2}$  is the OMI-measured tropospheric slant column  $\text{NO}_2$  and  $\text{AMF}_{\text{LNO}_x}$  is a customized lightning air mass factor.  $\text{AMF}_{\text{LNO}_x}$  is defined as the ratio of the "visible" modeled  $\text{NO}_2$  slant column to the total modeled tropospheric  $\text{LNO}_x$  vertical column (derived from the a priori  $\text{NO}$  and  $\text{NO}_2$  profiles, scattering weights, and radiance cloud fraction):

$$\text{AMF}_{\text{LNO}_x} = \frac{(1 - f_r) \int_{p_{\text{surf}}}^{p_{\text{tp}}} w_{\text{clear}}(p) \text{NO}_2(p) dp + f_r \int_{p_{\text{cloud}}}^{p_{\text{tp}}} w_{\text{cloudy}}(p) \text{NO}_2(p) dp}{\int_{p_{\text{surf}}}^{p_{\text{tp}}} \text{LNO}_x(p) dp} \quad (2)$$

155 where  $f_r$  is the radiance cloud fraction,  $p_{\text{surf}}$  is the surface pressure,  $p_{\text{tp}}$  is the tropopause pressure,  $p_{\text{cloud}}$  is the cloud optical pressure (CP),  $w_{\text{clear}}$  and  $w_{\text{cloudy}}$  are respectively the pressure dependent scattering weights from the TOMRAD lookup table (Bucsela et al., 2013) for clear and cloudy parts, and  $\text{NO}_2(p)$  is the modeled  $\text{NO}_2$  vertical profile. Details of these standard parameters and calculation methods are given in Laughner et al. (2018a).  $\text{LNO}_x(p)$  is the  $\text{LNO}_x$  vertical profile calculated by the difference of vertical profiles between WRF-Chem simulations with and without lightning.

To compare our results with those of Pickering et al. (2016) and Lapierre et al. (2019), we calculate their  $\text{AMF}_{\text{LNO}_x \text{Clean}}$  and  
160  $\text{AMF}_{\text{NO}_2 \text{Vis}}$  respectively:

$$\text{AMF}_{\text{LNO}_x \text{Clean}} = \frac{(1 - f_r) \int_{p_{\text{surf}}}^{p_{\text{tp}}} w_{\text{clear}}(p) \text{LNO}_2(p) dp + f_r \int_{p_{\text{cloud}}}^{p_{\text{tp}}} w_{\text{cloudy}}(p) \text{LNO}_2(p) dp}{\int_{p_{\text{surf}}}^{p_{\text{tp}}} \text{LNO}_x(p) dp} \quad (3)$$

$$\text{AMF}_{\text{NO}_2 \text{Vis}} = \frac{(1 - f_r) \int_{p_{\text{surf}}}^{p_{\text{tp}}} w_{\text{clear}}(p) \text{NO}_2(p) dp + f_r \int_{p_{\text{cloud}}}^{p_{\text{tp}}} w_{\text{cloudy}}(p) \text{NO}_2(p) dp}{(1 - f_g) \int_{p_{\text{surf}}}^{p_{\text{tp}}} \text{NO}_2(p) dp + f_g \int_{p_{\text{cloud}}}^{p_{\text{tp}}} \text{NO}_2(p) dp} \quad (4)$$

165 where  $f_g$  is the geometric cloud fraction and  $\text{LNO}_2(p)$  is the modeled  $\text{LNO}_2$  vertical profile. Besides these AMFs, another AMF called  $\text{AMF}_{\text{LNO}_2 \text{Vis}}$  is developed for comparison later. A full list of definitions of the used AMFs is shown in Appendix A.

$$\text{AMF}_{\text{LNO}_2 \text{Vis}} = \frac{(1 - f_r) \int_{p_{\text{surf}}}^{p_{\text{tp}}} w_{\text{clear}}(p) \text{NO}_2(p) dp + f_r \int_{p_{\text{cloud}}}^{p_{\text{tp}}} w_{\text{cloudy}}(p) \text{NO}_2(p) dp}{(1 - f_g) \int_{p_{\text{surf}}}^{p_{\text{tp}}} \text{LNO}_2(p) dp + f_g \int_{p_{\text{cloud}}}^{p_{\text{tp}}} \text{LNO}_2(p) dp} \quad (5)$$

170 Additionally, Vasilkov et al. (2008) found that  $p_{\text{cloud}}$ , retrieved by the OMI  $\text{O}_2\text{-O}_2$  algorithm (Bucsela et al., 2013), is often significantly larger than the IR-derived cloud top. This means that the back-scattered UV-VIS light observed by OMI penetrates deeper into the cloud. As a result, part of the  $\text{NO}_2$  originated from lightning can be detected by the OMI satellite. As discussed in Pickering et al. (2016), the ratio of  $V_{\text{LNO}_2}$  seen by OMI to  $V_{\text{LNO}_x}$  is partly influenced by  $p_{\text{cloud}}$ . The effects of  $\text{LNO}_2$  below the cloud will be discussed in section 3.3.

## 2.5 Procedures for Deriving $\text{LNO}_x$

175  $\text{LNO}_x$  is re-gridded to  $0.05^\circ \times 0.05^\circ$  pixels like the BEHR product and is analyzed in  $1^\circ \times 1^\circ$  grid boxes with a minimum of fifty valid pixels which is equivalent to five satellite pixels in Pickering et al. (2016). The main procedures used to derive  $\text{LNO}_x$  are as follows:

CRFs (CRFs  $\geq 70\%$ , CRFs  $\geq 90\%$  and CRFs = 100%) and CP  $\leq 650$  hPa are various criteria of deep convective clouds for OMI pixels (Ziemke et al., 2009; Choi et al., 2014; Pickering et al., 2016). The effect of different CRFs on the retrieved



LNO<sub>x</sub> is explored in section 3.2. Furthermore, another criterion of cloud fractions (CFs) is applied to the WRF-Chem results  
180 for the successful simulation of convections. The CFs are defined as the maximum cloud fraction calculated by the Xu-Randall  
method between 350 and 400 hPa (Xu and Randall, 1996). This atmospheric layer (between 350 and 400 hPa) avoids any  
biases in the simulation of high clouds. We choose CFs  $\geq 40\%$  suggested by Strode et al. (2017) to determine cloudy or clear  
for each simulation grid.

Besides properties of cloud, the time period and sufficient flashes (or strokes) are required for fresh LNO<sub>x</sub> detected by OMI.  
185 The time window ( $t_{\text{window}}$ ) is the hours prior to the OMI overpass time.  $t_{\text{window}}$  is limited to 2.4 h by the mean wind speed at  
pressure levels 500 – 100 hPa during OMI overpass time and the square root of the  $1^\circ \times 1^\circ$  box over the CONUS (Lapierre  
et al., 2019). Meanwhile, 2400 flashes  $\text{box}^{-1}$  and 8160 strokes  $\text{box}^{-1}$  are chosen as sufficient for detecting LNO<sub>x</sub> (Lapierre  
et al., 2019).

To ensure that lightning flashes are simulated successfully by WRF-Chem, the threshold of simulated total lightning flashes  
190 (TL) per box is set to 1000, which is fewer than that used by the ENTLN lightning observation, considering the uncertainty  
of lightning parameterization. In view of other NO<sub>2</sub> sources except LNO<sub>2</sub>, the ratio of modeled lightning NO<sub>2</sub> above cloud  
(LNO<sub>2</sub>Vis) to modeled NO<sub>2</sub> above cloud (NO<sub>2</sub>Vis) is defined to check whether enough LNO<sub>2</sub> can be detected by OMI. The  
ratio  $\geq 50\%$  indicates that LNO<sub>2</sub> is not polluted much above the cloud.

Finally, the NO<sub>2</sub> lifetime against oxidation should be taken into account. As estimated by Nault et al. (2016), the lifetime ( $\tau$ )  
195 of NO<sub>2</sub> in the near field of convections is  $\sim 3$  h. The initial value of NO<sub>2</sub> is solved by Eq. 6 as

$$NO_2(0) = NO_2(OMI) \times e^{0.5t/\tau} \quad (6)$$

where  $NO_2(0)$  is the moles of NO<sub>2</sub> emitted at time  $t = 0$ ,  $NO_2(OMI)$  is the moles of NO<sub>2</sub> measured at the OMI overpass  
time and  $0.5t$  is the half cross grid time which is 1.2 h, assuming that lightning occurred at the center of each  $1^\circ \times 1^\circ$  box.  
For each grid box, the mean LNO<sub>x</sub> vertical column is obtained by averaging  $V_{LNO_x}$  values from all regridded  $0.05^\circ \times 0.05^\circ$   
200 pixels in the box. This mean value is converted to moles LNO<sub>x</sub> using the dimensions of the grid box. Two methods are applied  
to estimate the seasonal mean LNO<sub>2</sub>/flash, LNO<sub>x</sub>/flash, LNO<sub>2</sub>/stroke and LNO<sub>x</sub>/stroke:

- (1) summation method: dividing the sum of LNO<sub>x</sub> by the sum of flashes (or strokes) in each  $1^\circ \times 1^\circ$  box in MJJA 2014;
- (2) linear regression method: applying the linear regression to daily summations of LNO<sub>x</sub> and flashes (or strokes).

### 3 Results

#### 205 3.1 Criteria Determination

To determine the suitable criteria from conditions defined in section 2.5, six different combinations are defined (Table 1) and  
applied to the original data with a linear regression method (Fig. 2).

A daily search of NO<sub>2</sub> product for coincident ENTLN flash (stroke) data results in 99 (102) valid days under the condition  
of CRF  $\geq 90\%$ . Taking the flashes type ENTLN data as an example, the number of valid days decreases from 99 to 81 under  
210 the basic condition coupled with TL  $\geq 1000$  and ratio  $\geq 50\%$ , while LNO<sub>x</sub>/flash increases from  $86.0 \pm 14.0$  mol/flash to  $114.8$



± 18.2 mol/flash. The result is almost the same as the one without ratio  $\geq 50\%$ . Although this indicates the criterion of TL works well, it is better to include the ratio in case of some exceptions in the different AMF methods. Since CF  $\geq 40\%$  leads to a sharp loss of valid numbers and production, therefore, it is not a suitable criterion. Instead the CRF criteria are used. Finally, coincident ENTLN data, TL  $\geq 1000$  and ratio  $\geq 50\%$  are chosen as the thresholds to explore the effects of three different CRF conditions (CRF  $\geq 70\%$ , CRF  $\geq 90\%$  and CRF = 100%) on LNO<sub>x</sub> production (Table 2).

Apart from the fewer valid days under higher CRF conditions (CRF  $\geq 90\%$  and CRF = 100%), LNO<sub>x</sub>/flash increases from 109.0 ± 15.3 mol/flash to 114.8 ± 18.2 mol/flash and decreases again to 99.4 ± 15.3 mol/flash while LNO<sub>x</sub>/stroke enhances from 16.7 ± 2.6 mol/stroke to 17.8 ± 2.9 mol/stroke and drops again to 15.6 ± 3.1 mol/stroke (Table 2). Although enhanced NO<sub>x</sub> is often observed in regions with CRF > 70% (Pickering et al., 2016), the following analysis will be based on the criterion of CRF  $\geq 90\%$  considering the contamination by low and mid-level NO<sub>2</sub> and comparisons with former studies.

### 3.2 Comparison of LNO<sub>x</sub> Production based on Different AMFs

Lapierre et al. (2019) derived LNO<sub>2</sub> production based on the BEHR NO<sub>2</sub> product. In order for our results to be comparable with those of Pickering et al. (2016) and Lapierre et al. (2019), we choose NO<sub>2</sub> instead of NO<sub>x</sub> to derive productions. In Fig. 3, time series of NO<sub>2</sub>Vis, LNO<sub>2</sub>Vis, LNO<sub>2</sub> and LNO<sub>2</sub>Clean production per day over CONUS are plotted for MJJA 2014 with the criterion of CRF  $\geq 90\%$  and a flash threshold of 2400 flashes per 2.4 h. LNO<sub>2</sub> productions are mostly in the range from 20 to 80 mol/flash. LNO<sub>2</sub>Vis productions are smaller than LNO<sub>2</sub> productions which contain LNO<sub>2</sub> below clouds. The simulation of GMI in Pickering et al. (2016) indicated that 25% – 30% of the LNO<sub>x</sub> column lies below the CP, while the ratio in our WRF-Chem simulation is 10% – 80%. The effect of clouds properties on LNO<sub>x</sub> production will be discussed in more detail in section 3.3. Generally, the order of estimated daily production efficiencies (PEs) is LNO<sub>2</sub>Clean > LNO<sub>2</sub> > NO<sub>2</sub>Vis > LNO<sub>2</sub>Vis. The percent difference in the estimated PE ( $\Delta$ PE) between NO<sub>2</sub>Vis and LNO<sub>2</sub>Vis indicates a certain amount of background NO<sub>2</sub> exists above clouds. Overall, the tendency of that  $\Delta$ PE is consistent with another  $\Delta$ PE between NO<sub>2</sub>Vis and LNO<sub>2</sub>Clean. When the region is highly polluted ( $\Delta$ PE between NO<sub>2</sub>Vis and LNO<sub>2</sub> is larger than 200%), PEs based on NO<sub>2</sub>Vis and LNO<sub>2</sub>Clean are significantly overestimated. In other words, NO<sub>2</sub>Vis and LNO<sub>2</sub>Clean are more sensitive to background NO<sub>2</sub>. The extent of the overestimation of NO<sub>2</sub>Vis is larger than that of LNO<sub>2</sub>Clean in highly polluted regions, while it is usually opposite in most regions.

Figure 4 shows the linear regression for ENTLN data versus NO<sub>2</sub>Vis, LNO<sub>2</sub>Vis, LNO<sub>2</sub> and LNO<sub>2</sub>Clean with the same criteria as shown in Fig. 3. LNO<sub>2</sub>Clean production (the largest slope) is 49.1 ± 8.4 mol NO<sub>2</sub>/flash with a correlation of 0.79 and 7.5 ± 1.3 mol NO<sub>2</sub>/stroke with a correlation of 0.77. As shown in Fig. 3, the number of positive percent differences between NO<sub>2</sub>Vis and LNO<sub>2</sub>Clean production is much fewer than that of negative differences. As a result, NO<sub>2</sub>Vis production (19.3 ± 2.7 mol NO<sub>2</sub>/flash and 3.6 ± 0.5 mol NO<sub>2</sub>/stroke) is smaller than LNO<sub>2</sub>Clean production using the linear regression method.

If the CP  $\leq 650$  hPa, TL  $\geq 1000$  and ratio  $\geq 50\%$  are removed from criteria, our result based on NO<sub>2</sub>Vis (3.8 ± 0.5 mol/stroke) is still larger than the value of 1.6 ± 0.1 mol/stroke mentioned in Lapierre et al. (2019). This may be caused by the different version of BEHR algorithm, as Lapierre et al. (2019) used BEHR V3.0A and our algorithm is based on BEHR V3.0B





245 (Laughner et al., 2019). The input of  $S_{\text{NO}_2}$  in both versions is from the NASA standard product V3 and the major improvements of BEHR V3.0B are listed below:

1. The profile (V3.0B) closest to the OMI overpass time was selected instead of the last profile (V3.0A) before the OMI overpass.

2. The AMF uses a variable tropopause height as opposed to the fixed 200 hPa tropopause.

250 3. The surface pressure is now calculated according to Zhou et al. (2009).

The detailed log of changes is available at <https://github.com/CohenBerkeleyLab/BEHR-core> (last access: November 26, 2019). Note that Lapierre et al. (2019) used the monthly  $\text{NO}_2$  profile, while the daily profile is used in our study and the interval of our outputs from WRF-Chem is 30 min which is more frequent than 1 h in the BEHR daily product, the AMF could be affected by different  $\text{NO}_2$  profiles. In view of these factors, we compare different methods based on our data to minimize  
255 these effects.

Meanwhile,  $\text{LNO}_2$  production ( $41.6 \pm 6.9$  mol/flash and  $6.3 \pm 1.1$  mol/stroke) is between  $\text{LNO}_2$  Clean production and  $\text{NO}_2$  Vis production, which coincides with the daily results in Fig. 3. Furthermore, the calculated  $\text{LNO}_x$  production is  $114.8 \pm 18.2$  mol/flash (or  $17.8 \pm 2.9$  mol/stroke) which is larger than 91 mol/flash from the linear regression result of Pickering et al. (2016), possibly due to the differences in geographic location, lightning data, chemistry model and the ratio of CG to IC  
260 considered by Pickering et al. (2016) and this study.

The mean and standard deviation of  $\text{LNO}_2$  production under  $\text{CRF} \geq 90\%$  using the summation method is  $46.2 \pm 35.1$  mol/flash and  $9.9 \pm 8.1$  mol/stroke, while  $\text{LNO}_x$  production is  $125.6 \pm 95.9$  mol/flash and  $26.7 \pm 21.6$  mol/stroke (Fig. 5). The  $\text{LNO}_2$  and  $\text{LNO}_x$  production are both higher in the South Central U.S. ( $88^\circ\text{W} - 103^\circ\text{W}$ ,  $28.5^\circ\text{N} - 39^\circ\text{N}$ ) and Southeast U.S. ( $79^\circ\text{W} - 85^\circ\text{W}$ ,  $25^\circ\text{N} - 35^\circ\text{N}$ ), consistent with Lapierre et al. (2019) and Bucsele et al. (2019). Compared with Fig. 3, Fig.  
265 6 (a) and (b) present some large differences between  $\text{NO}_2$  Vis production and  $\text{LNO}_2$  Vis production, which are consistent with what we expect for polluted regions. Meanwhile, the differences between  $\text{LNO}_2$  production and  $\text{NO}_2$  Vis production depend on background  $\text{NO}_2$ , the strength of updraft and the profile. The negative differences are caused by background  $\text{NO}_2$  carried by the updraft while parts of the below-cloud  $\text{LNO}_2$  results in more  $\text{LNO}_2$  production than  $\text{NO}_2$  Vis production (Fig. 6 c). Figure 6 (d) shows that the ratio of  $\text{LNO}_2$  Vis to  $\text{LNO}_2$  ranges from 10% – 80%. This may be caused by the height of the clouds and  
270 the profile of  $\text{LNO}_2$ . If the CP is near 300 hPa, the ratio should be smaller because of the coverage of clouds. The ratio would present the same trend while the peaks of  $\text{LNO}_2$  profile is below the CP. Therefore, a better understanding of  $\text{LNO}_2$  and  $\text{LNO}_x$  below clouds is required.

### 3.3 Effects of Cloud and $\text{LNO}_x$ Parameterization on $\text{LNO}_x$ Production

Figure 7 presents the daily distribution of CP and the ratio of  $\text{LNO}_2$  Vis to  $\text{LNO}_2$  during MJJA 2014 with the criteria defined in  
275 section 3.1 under  $\text{CRF} \geq 90\%$ . Since the ratio of  $\text{LNO}_2$  Vis to  $\text{LNO}_2$  decreases from 0.8 to 0.2 while the cloud is higher (smaller pressure value),  $\text{NO}_2$  Vis production is smaller than  $\text{LNO}_2$  in relatively clean areas as shown in Fig. 4. Apart from  $\text{LNO}_2$  Vis, the  $\text{LNO}_2$  production is also affected by CP. For  $\text{LNO}_2$  production larger than 30 mol/stroke, the CPs are all smaller than 550 hPa (Fig. 8). However, smaller  $\text{LNO}_2$  productions ( $< 30$  mol/stroke) occur on all levels between 650 hPa and 200 hPa. Because



of the limited amount of large LNO<sub>2</sub> production and lightning data, we can not derive that higher LNO<sub>2</sub> production relates to  
280 higher clouds or different lightning properties at this stage. Because CP only represents the development of clouds, the vertical  
structure of flashes can not be derived from the CP values only. As discussed in several previous studies, flash channel length  
varies and depends on the environmental conditions (Carey et al., 2016; Mecikalski and Carey, 2017; Fuchs and Rutledge,  
2018). Davis et al. (2019) compared two kinds of flashes: normal flashes and anomalous flashes. Because updrafts are stronger  
and flash rates are larger in anomalous storms, UT LNO<sub>x</sub> production is larger than normal polarity storms. In general, normal  
285 flashes are coupled with an upper-level positive charge region and a mid-level negative charge region, while anomalous flashes  
are opposite (Williams, 1989). It is not straightforward to estimate the error resulting from the vertical distribution of LNO<sub>x</sub>.  
There are mainly two methods of distributing LNO<sub>x</sub> in models: LNO<sub>x</sub> profiles (postconvection) are simulated after LNO<sub>x</sub> is  
redistributed by convective transport, while the other one (preconvection) uses LNO<sub>x</sub> profiles made before the redistribution of  
convective transport (Luo et al., 2017). However, given the similarity of results compared to other LNO<sub>x</sub> studies, we believe  
290 that our 1° × 1° results based on postconvective LNO<sub>x</sub> profile are sufficient for estimating average LNO<sub>x</sub> production.

The LNO production settings in WRF-Chem varied in different studies. Zhao et al. (2009) set a NO<sub>x</sub> production rate of  
250 mol NO per flash in a regional-scale model, while Bela et al. (2016) chose the same method (330 mol NO per flash)  
that was used by Barth et al. (2012). Wang et al. (2015) assumed approximately 500 mol NO per flash which was derived  
by a cloud-scale chemical transport model and in-cloud aircraft observations (Ott et al., 2010). To illustrate the impact of  
295 LNO<sub>x</sub> parameterization on LNO<sub>x</sub> estimation, we apply another WRF-Chem NO<sub>2</sub> profile setting (2×base flashrate, 500 mol  
NO flash<sup>-1</sup>; hereinafter referred to as "2×500 mol NO flash<sup>-1</sup>") to a priori profiles and evaluate the changes in AMF<sub>LNO<sub>2</sub></sub>,  
AMF<sub>LNO<sub>x</sub></sub>, LNO<sub>2</sub> and LNO<sub>x</sub> productions. For the linear regression method (Fig. 9), LNO<sub>2</sub> production is 46.4 ± 7.8 mol/flash  
which is 11.5% larger than the basic one (41.6 ± 6.9 mol/flash). However, LNO<sub>x</sub> production (increasing from 114.8 ± 18.2  
mol/flash to 143.4 ± 24.0 mol/flash) depends to a large extent on the configuration of LNO production in WRF-Chem (Fig.  
300 10). It remains unclear as to whether the NO-NO<sub>2</sub>-O<sub>3</sub> cycle or other LNO<sub>x</sub> reservoirs accounts for the increment of LNO<sub>x</sub>  
production. This would need detailed source analysis in WRF-Chem and is beyond the scope of this study.

Figure 11 shows the average percentage changes in AMF<sub>LNO<sub>2</sub></sub>, AMF<sub>LNO<sub>x</sub></sub>, LNO<sub>2</sub> and LNO<sub>x</sub> between retrievals using profiles  
based on 1×200 mol NO flash<sup>-1</sup> and 2×500 mol NO flash<sup>-1</sup>. These results were obtained by averaging data over MJJA 2014  
based on the method described in Sect. 2.5 with the criterion of CRF ≥ 90%. The effects on LNO<sub>2</sub> and LNO<sub>x</sub> retrieval from  
305 increasing LNO profile values show mostly the same tendency: smaller AMF<sub>LNO<sub>2</sub></sub> and AMF<sub>LNO<sub>x</sub></sub> leads to larger LNO<sub>2</sub> and  
LNO<sub>x</sub>, but the changes are region dependent. This is caused by the nonlinear calculation of AMF<sub>LNO<sub>2</sub></sub> and AMF<sub>LNO<sub>x</sub></sub>. As the  
contribution of LNO<sub>2</sub> increases, both the numerator and denominator of Eq. (2) increase. Note that the LNO<sub>2</sub> accounts for a  
fraction of NO<sub>2</sub> above the clouds, the magnitude of increasing denominator could be different in that of increasing numerator,  
resulting in a different effect on the AMF<sub>LNO<sub>2</sub></sub> and AMF<sub>LNO<sub>x</sub></sub>.

310 Figure 12 shows the comparison of the mean LNO and LNO<sub>2</sub> profiles in two specific regions where the 2×500 mol NO  
flash<sup>-1</sup> setting leads to both lower and higher LNO<sub>2</sub> production. The first one (Fig. 12a) is the region (36°N – 37°N, 89°W –  
90°W) containing the minimal negative percent change in LNO<sub>2</sub> (Fig. 11c). The second one (31°N – 32°N, 97°W – 98°W),  
Figure 12b, has the largest positive percent change in LNO<sub>2</sub> (Fig. 11c). Although the relative distribution of mean LNO



and LNO<sub>2</sub> profiles is similar in both regions, the magnitude differs with a factor of 10. This phenomenon implies that the  
315 performance of lightning parameterization in WRF-Chem is region dependent and the unrealistic profile could appear in the  
UT. Although this sensitivity analysis is false in some regions, it allows the calculation of an upper limit on the NO<sub>2</sub> due  
to LNO and LNO<sub>2</sub> profiles. As discussed in Laughner and Cohen (2017), the scattering weights are uniform under cloudy  
conditions and the sensitivity of NO<sub>2</sub> is nearly constant with different pressure levels because of the high albedo. However,  
the relative distribution of LNO<sub>2</sub> within the UT should be taken carefully in our research. If the LNO<sub>2</sub>/NO<sub>2</sub> above the cloud is  
320 large enough (Fig. 12a), the AMF<sub>LNO<sub>2</sub></sub> is largely determined by the ratio of LNO<sub>2</sub>Vis to LNO<sub>2</sub> which is related to the relative  
distribution. When the condition of high LNO<sub>2</sub>/NO<sub>2</sub> is not met, both relative distribution and ratio are involved (Fig. 12b).

To clarify this, we applied the same sensitivity test of different simulating LNO amounts for all four methods mentioned in  
Sect. 2.4: LNO<sub>2</sub>, LNO<sub>2</sub>Vis, LNO<sub>2</sub>Clean and NO<sub>2</sub>Vis (Fig. 13). Note that the threshold for CRF is set to 100% to simplify Eq.  
(2) to:

$$325 \quad AMF_{LNO_x} = \frac{\int_{p_{cloud}}^{p_{tp}} w_{cloudy}(p) NO_2(p) dp}{\int_{p_{surf}}^{p_{tp}} LNO_x(p) dp} \quad (7)$$

The overall differences of LNO<sub>2</sub>Clean and NO<sub>2</sub>Vis are smaller than those of LNO<sub>2</sub> and LNO<sub>2</sub>Vis. Comparing the composition  
of numerator and denominator in the equations, it is clear why the impact of different simulating LNO amounts is smaller in  
Fig. 13 (c) and (d). For LNO<sub>2</sub>Clean and NO<sub>2</sub>Vis, both the SCD and VCD will increase (decrease) when more (less) LNO<sub>2</sub>  
or NO<sub>2</sub> presents. The difference between Fig. 13(a) and Fig. 13(b) is the denominator: the total tropospheric LNO<sub>2</sub> vertical  
330 column and visible LNO<sub>2</sub> vertical column respectively. As a result, the negative values in Fig. 13(a) is caused by the part of  
LNO<sub>2</sub> below the cloud. The comparison between Figure 4 and Figure 9 shows that LNO<sub>2</sub>Clean and LNO<sub>2</sub> values are more  
similar while LNO<sub>2</sub> and NO<sub>2</sub>Vis values are same. The uncertainty of retrieved LNO<sub>2</sub> and LNO<sub>x</sub> productions is driven by this  
error, and we conservatively estimate this to be ± 13% and ± 26% respectively.

#### 4 Uncertainties Analysis

335 The uncertainties of the LNO<sub>2</sub> and LNO<sub>x</sub> production are estimated following Pickering et al. (2016), Lapierre et al. (2019) and  
Laughner et al. (2019). We determine the uncertainty due to BEHR tropopause pressure, cloud radiance fraction, surface pres-  
sure, surface reflectivity, profile shape, profile location, V<sub>strat</sub>, the detection efficiency of lightning, t<sub>window</sub> and LNO<sub>2</sub> lifetime  
numerically by perturbing each parameter in turn and re-retrieval of the LNO<sub>2</sub> and LNO<sub>x</sub> with the perturbed values (Table 3).

The GEOS-5 monthly tropopause pressure, which is consistent with the NASA Standard Product, is applied instead of the  
340 variable WRF tropopause height to evaluate the uncertainty (6% for LNO<sub>2</sub> and 4% for LNO<sub>x</sub>) caused by the BEHR tropopause  
pressure. The resolution of GLOBE terrain height data is much higher than the OMI pixel and a fixed scale height is assumed in  
the BEHR algorithm. As a result, Laughner et al. (2019) compared the average WRF surface pressures to the GLOBE surface  
pressures and arrived at the largest bias of 1.5%. Based on the largest bias, we vary the surface pressure (limited to less than  
1020 hPa) and the uncertainty can be neglected.



345 The error in cloud radiance fraction is transformed from cloud fraction using:

$$\sigma = 0.05 \cdot \left. \frac{\partial f_r}{\partial f_g} \right|_{f_{g, \text{pix}}} \quad (8)$$

where  $f_r$  is the cloud radiance fraction,  $f_g$  is the cloud fraction and  $f_{g, \text{pix}}$  is the cloud fraction of a specific pixel. We calculate  $\partial f_r / \partial f_g$  under  $f_{g, \text{pix}}$  by the relationship between all binned  $f_r$  and  $f_g$  with the increment of 0.05 for the each specific OMI orbit. Considering the relationship, the error in cloud fraction is converted to an error in cloud radiance fraction of 2% for both  
350 LNO<sub>2</sub> and LNO<sub>x</sub>.

The accuracy of the 500 m MODIS albedo product is usually within 5% of albedo observations at the validation sites and those exceptions with low quality flags have been found to be primarily within 10% of the field data (Schaaf et al., 2011). Since we use the bidirectional reflectance distribution function (BRDF) data directly, rather than including a radiative transfer model, 14% Lambertian equivalent reflectivity (LER) error and 10% uncertainty are combined to get a perturbation of 17% (Laughner  
355 et al., 2019). The uncertainty due to surface reflectivity can be neglected with the 17% perturbation.

As discussed at the end of Sect. 3.3, another setting of LNO<sub>2</sub> ( $2 \times 500 \text{ mol NO flash}^{-1}$ ) is applied to determine the uncertainty of the lightning parameterization and the vertical distribution of LNO in WRF-Chem. Differences between the two profiles lead to an uncertainty of 13% and 26% in the resulting LNO<sub>2</sub> and LNO<sub>x</sub> production. Another sensitivity test allows each pixel to shift by - 0.2, 0, or + 0.2 degrees in the directions of longitude and latitude, taking advantage of the high-resolution profile  
360 location in WRF-Chem. The resulting uncertainty of LNO<sub>x</sub> production is 1% including the error of transport and chemistry by shifting pixels.

Compared to the NASA standard product v2, Krotkov et al. (2017) demonstrated that the noise in  $V_{\text{strat}}$  is  $1 \times 10^{14} \text{ cm}^{-2}$ . Errors in polluted regions can be slightly larger than this value, while errors in the cleanest areas are typically significantly smaller (Bucsela et al., 2013). We estimated the uncertainty of  $V_{\text{strat}}$  component and the slant column errors to be 15% and 5%,  
365 respectively, following Allen et al. (2019).

Based on the standard deviation of the detection efficiency estimation over the CONUS relative to LIS, ENTLN detection efficiency uncertainties are  $\pm 16\%$  for total and IC flashes/strokes. Due to the high detection efficiency of CG over the CONUS, the uncertainty is estimated to be  $\pm 5\%$  (Lapierre et al., 2019). It is found that the resulting uncertainty of detection efficiency is 15% in the production analysis. We have used the  $t_{\text{window}}$  of 2.4 h for counting ENTLN flashes and strokes to analyze LNO<sub>2</sub> and  
370 LNO<sub>x</sub> production. Because  $t_{\text{window}}$  derived from the ERA5 reanalysis can not represent the variable wind speeds, a sensitivity test is performed which yields an uncertainty of 10% for production per flash and 8% for production per stroke using  $t_{\text{window}}$  of 2 h and 4 h. Meanwhile, the lifetime of UT NO<sub>x</sub> ranges from 2 hours to 12 hours depending on the convective location, the methyl peroxy nitrate and alkyl and multifunctional nitrates (Nault et al., 2017). The lifetime ( $\tau$ ) of NO<sub>2</sub> in Eq. (6) is replaced by 2 and 12 hours to determine the uncertainty as 24% due to lifetime. The lifetime is the most likely uncertainty in  
375 the production analysis of LNO<sub>2</sub> while the uncertainty caused by lightning parameterization is comparable with that for the LNO<sub>x</sub> type.

The overall uncertainty is estimated as the square root of the sum of the squares of all individual uncertainties in Table 3. The net uncertainty is 37% and 43% for LNO<sub>2</sub> type and LNO<sub>x</sub> type respectively. The mean LNO<sub>2</sub>/flash, LNO<sub>x</sub>/flash, LNO<sub>2</sub>/stroke,



LNO<sub>x</sub>/stroke based on the linear regression and summation method are 44 mol/flash, 120 mol/flash, 8 mol/stroke and 22  
380 mol/stroke. Applying the corresponding uncertainty to these mean values, we arrive at  $44 \pm 16$  mol LNO<sub>2</sub>/flash,  $120 \pm 52$  mol  
LNO<sub>x</sub>/flash,  $8 \pm 3$  mol LNO<sub>2</sub>/stroke and  $22 \pm 9$  mol LNO<sub>x</sub>/stroke. This is in the range of current literature estimate ranging  
from 33 to 500 mol LNO<sub>x</sub>/flash (Schumann and Huntrieser, 2007; Beirle et al., 2010; Bucselá et al., 2010). Bucselá et al. (2010)  
estimated LNO<sub>x</sub> production of 100 – 250 mol/flash which is similar to our flash-based results. Pickering et al. (2016) estimated  
385 LNO<sub>x</sub> production to be  $80 \pm 45$  mol per flash for the Gulf of Mexico, which is 50% smaller than our flash-based results over  
the CONUS. Note that the criteria defined in Sect. 3.1 lead to many missing data over the Gulf of Mexico, thus it is actually a  
comparison between different regions. For the stroke-based results, Lapierre et al. (2019) yields lower LNO<sub>2</sub> production of  $1.6$   
 $\pm 0.1$  mol per stroke, the difference is caused by the different version of BEHR algorithm and several settings as mentioned  
in Sect. 3.2. Bucselá et al. (2019) inferred an average value of  $200 \pm 110$  moles (67% larger than our results) LNO<sub>x</sub> produced  
per flash over the North America, this is related to the different algorithm and lightning data.

## 390 5 Conclusions

In this study, a new algorithm for retrieving LNO<sub>2</sub> (LNO<sub>x</sub>) from OMI, including LNO<sub>2</sub> (LNO<sub>x</sub>) below cloud, has been de-  
veloped for application over active convection, whether in clean or polluted regions. It uses specific criteria combining with  
several other conditions (sufficient CRF, coincident ENTLN data, TL  $\geq 1000$  and ratio  $\geq 50\%$ ) to ensure that the electrically  
active regions are detected by OMI and simulated by WRF-Chem successfully. We conducted an analysis on  $1^\circ \times 1^\circ$  daily  
395 boxes in MJJA 2014 and obtained the seasonal mean LNO<sub>2</sub> and LNO<sub>x</sub> PEs over the CONUS. Considering all the uncertainties  
(Table 3) and applying the summation and regression method, the final mean PEs are estimated to be  $44 \pm 16$  mol LNO<sub>2</sub>/flash,  
 $120 \pm 52$  mol LNO<sub>x</sub>/flash,  $8 \pm 3$  mol LNO<sub>2</sub>/stroke and  $22 \pm 9$  mol LNO<sub>x</sub>/stroke.

Compared with former methods, we find that NO<sub>2</sub>Vis and LNO<sub>2</sub>Clean are more sensitive to background NO<sub>2</sub>, while NO<sub>2</sub>Vis  
underestimates PE because of the neglected below-cloud LNO<sub>2</sub> and LNO<sub>2</sub>Clean overestimates LNO<sub>2</sub> production due to the  
400 over-cloud background NO<sub>2</sub>. Finally, implementing profiles generated with  $1 \times 200$  mol NO flash<sup>-1</sup> and  $2 \times 500$  mol NO  
flash<sup>-1</sup>, we find that the regionally dependent effect. Both the relative distribution of LNO<sub>2</sub> and the ratio of LNO<sub>2</sub> to NO<sub>2</sub>  
would take the comprehensive effect for differences by the nonlinear calculation of AMF<sub>LNO<sub>2</sub></sub> and AMF<sub>LNO<sub>x</sub></sub>.

Since other regions, like China and India, have much more NO<sub>2</sub> pollutions than the CONUS, it is necessary to consider the  
background NO<sub>2</sub> in detail. These analyses will be complemented by the recently launched satellite instrument (TROPOspheric  
405 Monitoring Instrument [TROPOMI]) (Veefkind et al., 2012; Boersma et al., 2018; Griffin et al., 2019) and Lightning Mapping  
Imager (LMI) on the new generation Chinese geostationary meteorological satellites Fengyun-4 (Min et al., 2017; Yang et al.,  
2017; Zhang et al., 2019). Future work investigating the flash channel length and more detailed lightning parameterization in  
WRF-Chem would greatly benefit LNO<sub>x</sub> estimation. Applying current method in future studies may enhance the accuracy of  
LNO<sub>x</sub> production at both local and global level.



410 *Code and data availability.* The retrieval algorithm used in Sect. 2.4 is available at <https://github.com/zxdawn/BEHR-LNOx> (last access: November 26, 2019; Zhang and Laughner, 2019). The WRF-Chem model output and LNO<sub>x</sub> product are available upon request to Xin Zhang (xinzhang1215@gmail.com).

## Appendix A: AMF Definitions used in this Study

$$AMF_{LNO_2} = \frac{(1 - f_r) \int_{p_{surf}}^{p_{tp}} w_{clear}(p) NO_2(p) dp + f_r \int_{p_{cloud}}^{p_{tp}} w_{cloudy}(p) NO_2(p) dp}{\int_{p_{surf}}^{p_{tp}} LNO_2(p) dp} \quad (A1)$$

$$415 \quad AMF_{LNO_x} = \frac{(1 - f_r) \int_{p_{surf}}^{p_{tp}} w_{clear}(p) NO_2(p) dp + f_r \int_{p_{cloud}}^{p_{tp}} w_{cloudy}(p) NO_2(p) dp}{\int_{p_{surf}}^{p_{tp}} LNO_x(p) dp} \quad (A2)$$

where  $f_r$  is the radiance cloud fraction,  $p_{surf}$  is the surface pressure,  $p_{tp}$  is the tropopause pressure,  $p_{cloud}$  is the cloud optical pressure (CP),  $w_{clear}$  and  $w_{cloudy}$  are respectively the pressure dependent scattering weights from the TOMRAD lookup table (Bucsela et al., 2013) for clear and cloudy parts, and  $NO_2(p)$  is the modeled NO<sub>2</sub> vertical profile.  $LNO_2(p)$  and  $LNO_x(p)$  are respectively the LNO<sub>2</sub> and LNO<sub>x</sub> vertical profile calculated by the difference of vertical profiles between WRF-Chem  
 420 simulations with and without lightning.

$$AMF_{LNO_2 Clean} = \frac{(1 - f_r) \int_{p_{surf}}^{p_{tp}} w_{clear}(p) LNO_2(p) dp + f_r \int_{p_{cloud}}^{p_{tp}} w_{cloudy}(p) LNO_2(p) dp}{\int_{p_{surf}}^{p_{tp}} LNO_2(p) dp} \quad (A3)$$

$$AMF_{NO_2 Vis} = \frac{(1 - f_r) \int_{p_{surf}}^{p_{tp}} w_{clear}(p) NO_2(p) dp + f_r \int_{p_{cloud}}^{p_{tp}} w_{cloudy}(p) NO_2(p) dp}{(1 - f_g) \int_{p_{surf}}^{p_{tp}} NO_2(p) dp + f_g \int_{p_{cloud}}^{p_{tp}} NO_2(p) dp} \quad (A4)$$

$$AMF_{NO_x Vis} = \frac{(1 - f_r) \int_{p_{surf}}^{p_{tp}} w_{clear}(p) NO_2(p) dp + f_r \int_{p_{cloud}}^{p_{tp}} w_{cloudy}(p) NO_2(p) dp}{(1 - f_g) \int_{p_{surf}}^{p_{tp}} NO_x(p) dp + f_g \int_{p_{cloud}}^{p_{tp}} NO_x(p) dp} \quad (A5)$$

$$AMF_{LNO_2 Vis} = \frac{(1 - f_r) \int_{p_{surf}}^{p_{tp}} w_{clear}(p) NO_2(p) dp + f_r \int_{p_{cloud}}^{p_{tp}} w_{cloudy}(p) NO_2(p) dp}{(1 - f_g) \int_{p_{surf}}^{p_{tp}} LNO_2(p) dp + f_g \int_{p_{cloud}}^{p_{tp}} LNO_2(p) dp} \quad (A6)$$

425 where  $f_g$  is the geometric cloud fraction and  $NO_x(p)$  is the modeled NO<sub>x</sub> vertical profile.

*Author contributions.* YY directed the research and RJvdA, XZ and YY designed the research with feedback from the other co-authors; RJvdA and XZ developed the algorithm; JLL provided guidance and supporting data on the ENTLN data; XZ performed simulations and analysis with the help of YY, RJvdA, QC, XK, SY, JC, CH and RS; YY, RJvdA, JLL and XZ interpreted the data and discussed the results. XZ drafted the manuscript with comments from the co-authors; JLL, RJvdA and YY edited the manuscript.



430 *Competing interests.* The authors declare that they have no conflict of interest.

*Acknowledgements.* This work was funded by the National Natural Science Foundation of China (91644224 and 41705118). We acknowledge use of the computational resource provided by the National Supercomputer Centre in Guangzhou (NSCC-GZ). We thank the University of California Berkeley Satellite Group for the basic BEHR algorithm. We also thank Earth Networks Company for providing the Earth Networks Total Lightning Network (ENTLN) datasets. We appreciate the discussions with Joshua L. Laughner for BEHR codes and  
435 Mary Barth for the WRF-Chem lightning NO<sub>x</sub> module. MOZART-4 global model output is available at <https://www.acom.ucar.edu/wrf-chem/mozart.shtml> (last access: November 26, 2019).



## References

- Allen, D. J., Pickering, K. E., Duncan, B. N., and Damon, M.: Impact of lightning NO emissions on North American photochemistry as determined using the Global Modeling Initiative (GMI) model, *Journal of Geophysical Research*, 115, 4711, 440 <https://doi.org/10.1029/2010JD014062>, 2010.
- Allen, D. J., Pickering, K. E., Bucseba, E. J., Krotkov, N., and Holzworth, R.: Lightning NO<sub>x</sub> Production in the Tropics as Determined Using OMI NO<sub>2</sub> Retrievals and WWLLN Stroke Data, *Journal of Geophysical Research: Atmospheres*, <https://doi.org/10.1029/2018JD029824>, 2019.
- Banerjee, A., Archibald, A. T., Maycock, A. C., Telford, P., Abraham, N. L., Yang, X., Braesicke, P., and Pyle, J. A.: Lightning NO<sub>x</sub>, a 445 key chemistry–climate interaction: impacts of future climate change and consequences for tropospheric oxidising capacity, *Atmospheric Chemistry and Physics*, 14, 9871–9881, <https://doi.org/10.5194/acp-14-9871-2014>, 2014.
- Barth, M. C., Lee, J., Hodzic, A., Pfister, G., Skamarock, W. C., Worden, J., Wong, J., and Noone, D.: Thunderstorms and upper troposphere chemistry during the early stages of the 2006 North American Monsoon, *Atmospheric Chemistry and Physics*, 12, 11 003–11 026, <https://doi.org/10.5194/acp-12-11003-2012>, 2012.
- 450 Beirle, S., Platt, U., Wenig, M., and Wagner, T.: NO<sub>x</sub> production by lightning estimated with GOME, *Advances in Space Research*, 34, 793–797, <https://doi.org/10.1016/j.asr.2003.07.069>, 2004.
- Beirle, S., Spichtinger, N., Stohl, A., Cummins, K. L., Turner, T., Boccippio, D., Cooper, O. R., Wenig, M., Grzegorski, M., Platt, U., and Wagner, T.: Estimating the NO<sub>x</sub> produced by lightning from GOME and NLDN data: A case study in the Gulf of Mexico, *Atmospheric Chemistry and Physics*, 6, 1075–1089, <https://doi.org/10.5194/acp-6-1075-2006>, 2006.
- 455 Beirle, S., Huntrieser, H., and Wagner, T.: Direct satellite observation of lightning-produced NO<sub>x</sub>, *Atmospheric Chemistry and Physics*, 10, 10965–10986, <https://doi.org/10.5194/acp-10-10965-2010>, 2010.
- Bela, M. M., Barth, M. C., Toon, O. B., Fried, A., Homeyer, C. R., Morrison, H., Cummings, K. A., Li, Y., Pickering, K. E., Allen, D. J., Yang, Q., Wennberg, P. O., Crouse, J. D., St. Clair, J. M., Teng, A. P., O’Sullivan, D., Huey, L. G., Chen, D., Liu, X., Blake, D. R., Blake, N. J., Apel, E. C., Hornbrook, R. S., Flocke, F., Campos, T., and Diskin, G.: Wet scavenging of soluble gases in DC3 deep 460 convective storms using WRF-Chem simulations and aircraft observations, *Journal of Geophysical Research: Atmospheres*, 121, 4233–4257, <https://doi.org/10.1002/2015JD024623>, 2016.
- Boersma, K. F., Eskes, H. J., Meijer, E. W., and Kelder, H. M.: Estimates of lightning NO<sub>x</sub> production from GOME satellite observations, *Atmospheric Chemistry and Physics*, 5, 2311–2331, <https://doi.org/10.5194/acp-5-2311-2005>, 2005.
- Boersma, K. F., Eskes, H. J., Richter, A., de Smedt, I., Lorente, A., Beirle, S., van Geffen, J. H. G. M., Zara, M., Peters, E., van Roozendaal, 465 M., Wagner, T., de Maasackers, J., van der A, R. J., Nightingale, J., de Rudder, A., Irie, H., Pinardi, G., Lambert, J.-C., and Compernelle, S. C.: Improving algorithms and uncertainty estimates for satellite NO<sub>2</sub> retrievals: results from the quality assurance for the essential climate variables (QA4ECV) project, *Atmospheric Measurement Techniques*, 11, 6651–6678, <https://doi.org/10.5194/amt-11-6651-2018>, 2018.
- Bovensmann, H., Burrows, J. P., Buchwitz, M., Frerick, J., Noël, S., Rozanov, V. V., Chance, K. V., and Goede, A. P. H.: SCIAMACHY: Mission Objectives and Measurement Modes, *Journal of the Atmospheric Sciences*, 56, 127–150, [https://doi.org/10.1175/1520-0469\(1999\)056<0127:SMOAMM>2.0.CO;2](https://doi.org/10.1175/1520-0469(1999)056<0127:SMOAMM>2.0.CO;2), 1999.
- 470 Browne, E. C., Wooldridge, P. J., Min, K.-E., and Cohen, R. C.: On the role of monoterpene chemistry in the remote continental boundary layer, *Atmospheric Chemistry and Physics*, 14, 1225–1238, <https://doi.org/10.5194/acp-14-1225-2014>, 2014.





- 475 Bucselá, E. J., Pickering, K. E., Huntemann, T. L., Cohen, R. C., Perring, A., Gleason, J. F., Blakeslee, R. J., Albrecht, R. I., Holzworth, R., Cipriani, J. P., Vargas-Navarro, D., Mora-Segura, I., Pacheco-Hernández, A., and Laporte-Molina, S.: Lightning-generated  $\text{NO}_x$  seen by the Ozone Monitoring Instrument during NASA's Tropical Composition, Cloud and Climate Coupling Experiment ( $\text{TC}^4$ ), *Journal of Geophysical Research*, 115, 793, <https://doi.org/10.1029/2009JD013118>, 2010.
- 480 Bucselá, E. J., Krotkov, N. A., Celarier, E. A., Lamsal, L. N., Swartz, W. H., Bhartia, P. K., Boersma, K. F., Veefkind, J. P., Gleason, J. F., and Pickering, K. E.: A new stratospheric and tropospheric  $\text{NO}_2$  retrieval algorithm for nadir-viewing satellite instruments: Applications to OMI, *Atmospheric Measurement Techniques*, 6, 2607–2626, <https://doi.org/10.5194/amt-6-2607-2013>, 2013.
- Bucselá, E. J., Pickering, K. E., Allen, D. J., Holzworth, R., and Krotkov, N. A.: Midlatitude lightning  $\text{NO}_x$  production efficiency inferred from OMI and WWLLN data, *Journal of Geophysical Research: Atmospheres*, <https://doi.org/10.1029/2019JD030561>, 2019.
- 485 Burrows, J. P., Weber, M., Buchwitz, M., Rozanov, V., Ladstätter-Weissenmayer, A., Richter, A., DeBeek, R., Hoogen, R., Bramstedt, K., Eichmann, K.-U., Eisinger, M., and Perner, D.: The Global Ozone Monitoring Experiment (GOME): Mission Concept and First Scientific Results, *Journal of the Atmospheric Sciences*, 56, 151–175, [https://doi.org/10.1175/1520-0469\(1999\)056<0151:TGOMEG>2.0.CO;2](https://doi.org/10.1175/1520-0469(1999)056<0151:TGOMEG>2.0.CO;2), 1999.
- Callies, J., Corpaccioli, E., Eisinger, M., Hahne, A., and Lefebvre, A.: GOME-2-Metop's second-generation sensor for operational ozone monitoring, *ESA bulletin*, 102, 28–36, 2000.
- Carey, L. D., Koshak, W., Peterson, H., and Mecikalski, R. M.: The kinematic and microphysical control of lightning rate, extent, and  $\text{NO}_x$  production, *Journal of Geophysical Research: Atmospheres*, 121, 7975–7989, <https://doi.org/10.1002/2015JD024703>, 2016.
- 490 Choi, S., Joiner, J., Choi, Y., Duncan, B. N., Vasilkov, A., Krotkov, N., and Bucselá, E.: First estimates of global free-tropospheric  $\text{NO}_2$  abundances derived using a cloud-slicing technique applied to satellite observations from the Aura Ozone Monitoring Instrument (OMI), *Atmospheric Chemistry and Physics*, 14, 10 565–10 588, <https://doi.org/10.5194/acp-14-10565-2014>, 2014.
- Clark, S. K., Ward, D. S., and Mahowald, N. M.: Parameterization-based uncertainty in future lightning flash density, *Geophysical Research Letters*, 44, 2893–2901, <https://doi.org/10.1002/2017GL073017>, 2017.
- 495 Davis, T. C., Rutledge, S. A., and Fuchs, B. R.: Lightning location,  $\text{NO}_x$  production, and transport by anomalous and normal polarity thunderstorms, *Journal of Geophysical Research: Atmospheres*, <https://doi.org/10.1029/2018JD029979>, 2019.
- DeCaria, A. J., Pickering, K. E., Stenchikov, G. L., Scala, J. R., Stith, J. L., Dye, J. E., Ridley, B. A., and Laroche, P.: A cloud-scale model study of lightning-generated  $\text{NO}_x$  in an individual thunderstorm during STERAO-A, *Journal of Geophysical Research*, 105, 11 601–11 616, <https://doi.org/10.1029/2000JD900033>, 2000.
- 500 DeCaria, A. J., Pickering, K. E., Stenchikov, G. L., and Ott, L. E.: Lightning-generated  $\text{NO}_x$  and its impact on tropospheric ozone production: A three-dimensional modeling study of a Stratosphere-Troposphere Experiment: Radiation, Aerosols and Ozone (STERAO-A) thunderstorm, *Journal of Geophysical Research*, 110, n/a–n/a, <https://doi.org/10.1029/2004JD005556>, 2005.
- Dobber, M., Kleipool, Q., Dirksen, R., Levelt, P., Jaross, G., Taylor, S., Kelly, T., Flynn, L., Leppelmeier, G., and Rozemeijer, N.: Validation of Ozone Monitoring Instrument level 1b data products, *Journal of Geophysical Research*, 113, 5224, <https://doi.org/10.1029/2007JD008665>, 505 2008.
- Emmons, L. K., Walters, S., Hess, P. G., Lamarque, J.-F., Pfister, G. G., Fillmore, D., Granier, C., Guenther, A., Kinnison, D., Laepple, T., Orlando, J., Tie, X., Tyndall, G., Wiedinmyer, C., Baughcum, S. L., and Kloster, S.: Description and evaluation of the Model for Ozone and Related chemical Tracers, version 4 (MOZART-4), *Geoscientific Model Development*, 3, 43–67, <https://doi.org/10.5194/gmd-3-43-2010>, 2010.
- 510 EPA, U. S. and OAR: Air Pollutant Emissions Trends Data | US EPA, <https://www.epa.gov/air-emissions-inventories/air-pollutant-emissions-trends-data>, 2015.



- Finney, D. L., Doherty, R. M., Wild, O., Young, P. J., and Butler, A.: Response of lightning NO<sub>x</sub> emissions and ozone production to climate change: Insights from the Atmospheric Chemistry and Climate Model Intercomparison Project, *Geophysical Research Letters*, 43, 5492–5500, <https://doi.org/10.1002/2016GL068825>, 2016.
- 515 Finney, D. L., Doherty, R. M., Wild, O., Stevenson, D. S., MacKenzie, I. A., and Blyth, A. M.: A projected decrease in lightning under climate change, *Nature Climate Change*, 8, 210–213, <https://doi.org/10.1038/s41558-018-0072-6>, 2018.
- Fried, A., Barth, M. C., Bela, M., Weibring, P., Richter, D., Walega, J., Li, Y., Pickering, K., Apel, E., Hornbrook, R., Hills, A., Riemer, D. D., Blake, N., Blake, D. R., Schroeder, J. R., Luo, Z. J., Crawford, J. H., Olson, J., Rutledge, S., Betten, D., Biggerstaff, M. I., Diskin, G. S., Sachse, G., Campos, T., Flocke, F., Weinheimer, A., Cantrell, C., Pollack, I., Peischl, J., Froyd, K., Wisthaler, A., Mikoviny, T., and Woods, S.: Convective transport of formaldehyde to the upper troposphere and lower stratosphere and associated scavenging in thunderstorms over the central United States during the 2012 DC3 study, *Journal of Geophysical Research: Atmospheres*, 121, 7430–7460, <https://doi.org/10.1002/2015JD024477>, 2016.
- 520 Fuchs, B. R. and Rutledge, S. A.: Investigation of Lightning Flash Locations in Isolated Convection Using LMA Observations, *Journal of Geophysical Research: Atmospheres*, 123, 6158–6174, <https://doi.org/10.1002/2017JD027569>, 2018.
- 525 Goliff, W. S., Stockwell, W. R., and Lawson, C. V.: The regional atmospheric chemistry mechanism, version 2, *Atmospheric Environment*, 68, 174–185, <https://doi.org/10.1016/j.atmosenv.2012.11.038>, 2013.
- Grell, G. A., Peckham, S. E., Schmitz, R., McKeen, S. A., Frost, G., Skamarock, W. C., and Eder, B.: Fully coupled “online” chemistry within the WRF model, *Atmospheric Environment*, 39, 6957–6975, <https://doi.org/10.1016/j.atmosenv.2005.04.027>, 2005.
- Griffin, D., Zhao, X., McLinden, C. A., Boersma, F., Bourassa, A., Dammers, E., Degenstein, D., Eskes, H., Fehr, L., Fioletov, V., Hayden, K., Kharol, S. K., Li, S.-M., Makar, P., Martin, R. V., Mihele, C., Mittermeier, R. L., Krotkov, N., Snee, M., Lamsal, L. N., Linden, M. t., van Geffen, J., Veefkind, P., and Wolde, M.: High-Resolution Mapping of Nitrogen Dioxide With TROPOMI: First Results and Validation Over the Canadian Oil Sands, *Geophysical Research Letters*, 46, 1049–1060, <https://doi.org/10.1029/2018GL081095>, 2019.
- 530 Guenther, A., Karl, T., Harley, P., Wiedinmyer, C., Palmer, P. I., and Geron, C.: Estimates of global terrestrial isoprene emissions using MEGAN (Model of Emissions of Gases and Aerosols from Nature), *Atmospheric Chemistry and Physics*, 6, 3181–3210, <https://hal.archives-ouvertes.fr/hal-00295995>, 2006.
- 535 Hauglustaine, D., Emmons, L., Newchurch, M., Brasseur, G., Takao, T., Matsubara, K., Johnson, J., Ridley, B., Stith, J., and Dye, J.: On the Role of Lightning NO<sub>x</sub> in the Formation of Tropospheric Ozone Plumes: A Global Model Perspective, *Journal of Atmospheric Chemistry*, 38, 277–294, <https://doi.org/10.1023/A:1006452309388>, 2001.
- Krause, A., Kloster, S., Wilkenskjaeld, S., and Paeth, H.: The sensitivity of global wildfires to simulated past, present, and future lightning frequency, *Journal of Geophysical Research: Biogeosciences*, 119, 312–322, <https://doi.org/10.1002/2013JG002502>, 2014.
- 540 Krotkov, N. A., Lamsal, L. N., Celarier, E. A., Swartz, W. H., Marchenko, S. V., Bucsela, E. J., Chan, K. L., Wenig, M., and Zara, M.: The version 3 OMI NO<sub>2</sub> standard product, *Atmospheric Measurement Techniques*, 10, 3133–3149, <https://doi.org/10.5194/amt-10-3133-2017>, 2017.
- Lapierre, J. L., Laughner, J. L., Geddes, J. A., Koshack, W., Cohen, R. C., and Pusede, S. E.: Observing regional variability in lightning NO<sub>x</sub> production rates, *Journal of Geophysical Research*, in review, 2019.
- 545 Laughner, J. L. and Cohen, R. C.: Quantification of the effect of modeled lightning NO<sub>2</sub> on UV–visible air mass factors, *Atmospheric Measurement Techniques*, 10, 4403–4419, <https://doi.org/10.5194/amt-10-4403-2017>, 2017.
- Laughner, J. L., Zhu, Q., and Cohen, R. C.: The Berkeley High Resolution Tropospheric NO<sub>2</sub> Product, *Earth System Science Data Discussions*, pp. 1–33, <https://doi.org/10.5194/essd-2018-66>, 2018a.



- 550 Laughner, J. L., Zhu, Q., and Cohen, R. C.: Evaluation of version 3.0B of the BEHR OMI NO<sub>2</sub> product, *Atmospheric Measurement Techniques Discussions*, pp. 1–25, <https://doi.org/10.5194/amt-2018-248>, 2018b.
- Laughner, J. L., Zhu, Q., and Cohen, R. C.: Evaluation of version 3.0B of the BEHR OMI NO<sub>2</sub> product, *Atmospheric Measurement Techniques*, 12, 129–146, <https://doi.org/10.5194/amt-12-129-2019>, 2019.
- Levelt, P. F., van den Oord, G., Dobber, M. R., Malkki, A., Visser, H., Vries, J. d., Stammes, P., Lundell, J., and Saari, H.: The ozone monitoring instrument, *IEEE Transactions on Geoscience and Remote Sensing*, 44, 1093–1101, <https://doi.org/10.1109/TGRS.2006.872333>, 2006.
- 555 Levelt, P. F., Joiner, J., Tamminen, J., Veefkind, J. P., Bhartia, P. K., Stein Zweers, D. C., Duncan, B. N., Streets, D. G., Eskes, H., van der A, R., McLinden, C., Fioletov, V., Carn, S., de Laat, J., DeLand, M., Marchenko, S., McPeters, R., Ziemke, J., Fu, D., Liu, X., Pickering, K., Apituley, A., González Abad, G., Arola, A., Boersma, F., Chan Miller, C., Chance, K., de Graaf, M., Hakkarainen, J., Hassinen, S., Ialongo, I., Kleipool, Q., Krotkov, N., Li, C., Lamsal, L., Newman, P., Nowlan, C., Suleiman, R., Tilstra, L. G., Torres, O., Wang, H., and Wargan, K.: The Ozone Monitoring Instrument: overview of 14 years in space, *Atmospheric Chemistry and Physics*, 18, 5699–5745, <https://doi.org/10.5194/acp-18-5699-2018>, 2018.
- 560 Li, Y., Pickering, K. E., Allen, D. J., Barth, M. C., Bela, M. M., Cummings, K. A., Carey, L. D., Mecikalski, R. M., Fierro, A. O., Campos, T. L., Weinheimer, A. J., Diskin, G. S., and Biggerstaff, M. I.: Evaluation of deep convective transport in storms from different convective regimes during the DC3 field campaign using WRF-Chem with lightning data assimilation, *Journal of Geophysical Research: Atmospheres*, 122, 7140–7163, <https://doi.org/10.1002/2017JD026461>, 2017.
- 565 Luo, C., Wang, Y., and Koshak, W. J.: Development of a self-consistent lightning NO<sub>x</sub> simulation in large-scale 3-D models, *Journal of Geophysical Research: Atmospheres*, 122, 3141–3154, <https://doi.org/10.1002/2016JD026225>, 2017.
- Martin, R. V., Sauvage, B., Folkens, I., Sioris, C. E., Boone, C., Bernath, P., and Ziemke, J.: Space-based constraints on the production of nitric oxide by lightning, *Journal of Geophysical Research*, 112, 1479, <https://doi.org/10.1029/2006JD007831>, 2007.
- 570 Mecikalski, R. M. and Carey, L. D.: Lightning characteristics relative to radar, altitude and temperature for a multicell, MCS and supercell over northern Alabama, *Atmospheric Research*, 191, 128–140, <https://doi.org/10.1016/j.atmosres.2017.03.001>, <http://www.sciencedirect.com/science/article/pii/S0169809516302812>, 2017.
- Min, M., Wu, C., Li, C., Liu, H., Xu, N., Wu, X., Chen, L., Wang, F., Sun, F., Qin, D., Wang, X., Li, B., Zheng, Z., Cao, G., and Dong, L.: Developing the science product algorithm testbed for Chinese next-generation geostationary meteorological satellites: Fengyun-4 series, *JOURNAL OF METEOROLOGICAL RESEARCH*, 31, 708–719, <https://doi.org/10.1007/s13351-017-6161-z>, 2017.
- 575 Myhre, G., Shindell, D., Bréon, F. M., Collins, W., Fuglestedt, J., Huang, J., Koch, D., Lamarque, J. F., Lee, D., and Mendoza, B.: Climate change 2013: the physical science basis. Contribution of Working Group I to the Fifth Assessment Report of the Intergovernmental Panel on Climate Change, K., Tignor, M., Allen, SK, Boschung, J., Nauels, A., Xia, Y., Bex, V., and Midgley, PM, Cambridge University Press
- 580 Cambridge, United Kingdom and New York, NY, USA, 2013.
- Nault, B. A., Garland, C., Wooldridge, P. J., Brune, W. H., Campuzano-Jost, P., Crounse, J. D., Day, D. A., Dibb, J., Hall, S. R., Huey, L. G., Jimenez, J. L., Liu, X., Mao, J., Mikoviny, T., Peischl, J., Pollack, I. B., Ren, X., Ryerson, T. B., Scheuer, E., Ullmann, K., Wennberg, P. O., Wisthaler, A., Zhang, L., and Cohen, R. C.: Observational Constraints on the Oxidation of NO<sub>x</sub> in the Upper Troposphere, *The Journal of Physical Chemistry A*, 120, 1468–1478, <https://doi.org/10.1021/acs.jpca.5b07824>, 2016.
- 585 Nault, B. A., Laughner, J. L., Wooldridge, P. J., Crounse, J. D., Dibb, J., Diskin, G., Peischl, J., Podolske, J. R., Pollack, I. B., Ryerson, T. B., Scheuer, E., Wennberg, P. O., and Cohen, R. C.: Lightning NO<sub>x</sub> Emissions: Reconciling Measured and Modeled Estimates With Updated NO<sub>x</sub> Chemistry, *Geophysical Research Letters*, 44, 9479–9488, <https://doi.org/10.1002/2017GL074436>, 2017.



- Ott, L. E., Pickering, K. E., Stenchikov, G. L., Huntrieser, H., and Schumann, U.: Effects of lightning NO<sub>x</sub> production during the 21 July European Lightning Nitrogen Oxides Project storm studied with a three-dimensional cloud-scale chemical transport model, *Journal of Geophysical Research*, 112, 61, <https://doi.org/10.1029/2006JD007365>, 2007.
- Ott, L. E., Pickering, K. E., Stenchikov, G. L., Allen, D. J., DeCaria, A. J., Ridley, B., Lin, R.-F., Lang, S., and Tao, W.-K.: Production of lightning NO<sub>x</sub> and its vertical distribution calculated from three-dimensional cloud-scale chemical transport model simulations, *Journal of Geophysical Research*, 115, 4711, <https://doi.org/10.1029/2009JD011880>, 2010.
- Pickering, K. E., Thompson, A. M., Wang, Y., Tao, W.-K., McNamara, D. P., Kirchhoff, V. W. J. H., Heikes, B. G., Sachse, G. W., Bradshaw, J. D., Gregory, G. L., and Blake, D. R.: Convective transport of biomass burning emissions over Brazil during TRACE A, *Journal of Geophysical Research*, 101, 23 993–24 012, <https://doi.org/10.1029/96JD00346>, 1996.
- Pickering, K. E., Bucsela, E., Allen, D., Ring, A., Holzworth, R., and Krotkov, N.: Estimates of lightning NO<sub>x</sub> production based on OMI NO<sub>2</sub> observations over the Gulf of Mexico, *Journal of Geophysical Research: Atmospheres*, 121, 8668–8691, <https://doi.org/10.1002/2015JD024179>, 2016.
- Platt, U. and Perner, D.: Measurements of Atmospheric Trace Gases by Long Path Differential UV/Visible Absorption Spectroscopy, in: *Optical and Laser Remote Sensing*, edited by Schawlow, A. L., Killinger, D. K., and Mooradian, A., vol. 39 of *Springer Series in Optical Sciences*, pp. 97–105, Springer Berlin Heidelberg, Berlin, Heidelberg, [https://doi.org/10.1007/978-3-540-39552-2\\_13](https://doi.org/10.1007/978-3-540-39552-2_13), 1983.
- Richter, A., Burrows, J. P., Nüß, H., Granier, C., and Niemeier, U.: Increase in tropospheric nitrogen dioxide over China observed from space, *Nature*, 437, 129–132, <https://doi.org/10.1038/nature04092>, 2005.
- Rudlosky, S.: Evaluating ENTLN performance relative to TRMM/LIS, *Journal of Operational Meteorology*, 3, 11–20, <https://doi.org/10.15191/nwajom.2015.0302>, 2015.
- Schaaf, C. B., Liu, J., Gao, F., and Strahler, A. H.: Aqua and Terra MODIS Albedo and Reflectance Anisotropy Products, in: *Land Remote Sensing and Global Environmental Change*, edited by Ramachandran, B., Justice, C. O., and Abrams, M. J., vol. 11 of *Remote Sensing and Digital Image Processing*, pp. 549–561, Springer New York, New York, NY, [https://doi.org/10.1007/978-1-4419-6749-7\\_24](https://doi.org/10.1007/978-1-4419-6749-7_24), 2011.
- Schumann, U. and Huntrieser, H.: The global lightning-induced nitrogen oxides source, *Atmospheric Chemistry and Physics*, 7, 3823–3907, <https://doi.org/10.5194/acp-7-3823-2007>, 2007.
- Schwantes, R. H., Teng, A. P., Nguyen, T. B., Coggon, M. M., Crouse, J. D., St Clair, J. M., Zhang, X., Schilling, K. A., Seinfeld, J. H., and Wennberg, P. O.: Isoprene NO<sub>3</sub> Oxidation Products from the RO<sub>2</sub> + HO<sub>2</sub> Pathway, *The Journal of Physical Chemistry A*, 119, 10 158–10 171, <https://doi.org/10.1021/acs.jpca.5b06355>, 2015.
- Strode, S. A., Douglass, A. R., Ziemke, J. R., Manyin, M., Nielsen, J. E., and Oman, L. D.: A Model and Satellite-Based Analysis of the Tropospheric Ozone Distribution in Clear Versus Convectively Cloudy Conditions, *Journal of Geophysical Research: Atmospheres*, 122, 11,948–11,960, <https://doi.org/10.1002/2017JD027015>, 2017.
- Vasilkov, A., Joiner, J., Spurr, R., Bhartia, P. K., Levelt, P., and Stephens, G.: Evaluation of the OMI cloud pressures derived from rotational Raman scattering by comparisons with other satellite data and radiative transfer simulations, *Journal of Geophysical Research*, 113, D05 204, <https://doi.org/10.1029/2007JD008689>, 2008.
- Veefkind, J. P., Aben, I., McMullan, K., Förster, H., de Vries, J., Otter, G., Claas, J., Eskes, H. J., de Haan, J. F., Kleipool, Q., van Weele, M., Hasekamp, O., Hoogeveen, R., Landgraf, J., Snel, R., Tol, P., Ingmann, P., Voors, R., Kruizinga, B., Vink, R., Visser, H., and Levelt, P. F.: TROPOMI on the ESA Sentinel-5 Precursor: A GMES mission for global observations of the atmospheric composition for climate, air quality and ozone layer applications, *Remote Sensing of Environment*, 120, 70–83, <https://doi.org/10.1016/j.rse.2011.09.027>, 2012.



- 625 Wang, L., Follette-Cook, M. B., Newchurch, M. J., Pickering, K. E., Pour-Biazar, A., Kuang, S., Koshak, W., and Peterson, H.: Evaluation of lightning-induced tropospheric ozone enhancements observed by ozone lidar and simulated by WRF/Chem, *Atmospheric Environment*, 115, 185–191, <https://doi.org/10.1016/j.atmosenv.2015.05.054>, 2015.
- Williams, E. R.: The tripole structure of thunderstorms, *Journal of Geophysical Research*, 94, 13 151, <https://doi.org/10.1029/JD094iD11p13151>, 1989.
- 630 Wong, J., Barth, M. C., and Noone, D.: Evaluating a lightning parameterization based on cloud-top height for mesoscale numerical model simulations, *Geoscientific Model Development*, 6, 429–443, <https://doi.org/10.5194/gmd-6-429-2013>, 2013.
- Xu, K.-M. and Randall, D. A.: A Semiempirical Cloudiness Parameterization for Use in Climate Models, *Journal of the Atmospheric Sciences*, 53, 3084–3102, [https://doi.org/10.1175/1520-0469\(1996\)053<3084:ASCPFU>2.0.CO;2](https://doi.org/10.1175/1520-0469(1996)053<3084:ASCPFU>2.0.CO;2), 1996.
- Yang, J., Zhang, Z., Wei, C., Lu, F., and Guo, Q.: Introducing the New Generation of Chinese Geostationary Weather Satellites, *Fengyun-4*,  
635 *Bulletin of the American Meteorological Society*, 98, 1637–1658, <https://doi.org/10.1175/BAMS-D-16-0065.1>, 2017.
- Zel'dovich, Y. and Raizer, Y.: VIII - Physical and chemical kinetics in hydrodynamic processes, in: *Physics of Shock Waves and High-Temperature Hydrodynamic Phenomena*, edited by Hayes, W. D., Probstein, R. F., Zel'dovich, Y., and Raizer, Y., pp. 566–571, Academic Press, <https://doi.org/10.1016/B978-0-12-395672-9.50009-6>, 1967.
- Zhang, P., Lu, Q., Hu, X., Gu, S., Yang, L., Min, M., Chen, L., Xu, N., Sun, L., Bai, W., Ma, G., and Di Xian: Latest Progress of the  
640 *Chinese Meteorological Satellite Program and Core Data Processing Technologies*, *Advances in Atmospheric Sciences*, 36, 1027–1045, <https://doi.org/10.1007/s00376-019-8215-x>, 2019.
- Zhang, X. and Laughner, J.: zxdawn/BEHR-LNOx: v1.0, Zenodo, <https://doi.org/10.5281/zenodo.3553426>, 2019.
- Zhao, C., Wang, Y., Choi, Y., and Zeng, T.: Summertime impact of convective transport and lightning NO<sub>x</sub> production over North America: modeling dependence on meteorological simulations, *Atmospheric Chemistry and Physics*, 9, 4315–4327, <https://doi.org/10.5194/acp-9-4315-2009>, 2009.  
645
- Zhou, Y., Brunner, D., Boersma, K. F., Dirksen, R., and Wang, P.: An improved tropospheric NO<sub>2</sub> retrieval for OMI observations in the vicinity of mountainous terrain, *Atmospheric Measurement Techniques*, 2, 401–416, <https://doi.org/10.5194/amt-2-401-2009>, 2009.
- Zhu, Y., Rakov, V. A., Tran, M. D., and Nag, A.: A study of National Lightning Detection Network responses to natural lightning based on ground truth data acquired at LOG with emphasis on cloud discharge activity, *Journal of Geophysical Research: Atmospheres*, 121,  
650 14,651–14,660, <https://doi.org/10.1002/2016JD025574>, 2016.
- Zhu, Y., Rakov, V. A., Tran, M. D., Stock, M. G., Heckman, S., Liu, C., Sloop, C. D., Jordan, D. M., Uman, M. A., Caicedo, J. A., Kotovsky, D. A., Wilkes, R. A., Carvalho, F. L., Ngin, T., Gamerota, W. R., Pilkey, J. T., and Hare, B. M.: Evaluation of ENTLN Performance Characteristics Based on the Ground Truth Natural and Rocket-Triggered Lightning Data Acquired in Florida, *Journal of Geophysical Research: Atmospheres*, 122, 9858–9866, <https://doi.org/10.1002/2017JD027270>, 2017.
- 655 Ziemke, J. R., Joiner, J., Chandra, S., Bhartia, P. K., Vasilkov, A., Haffner, D. P., Yang, K., Schoeberl, M. R., Froidevaux, L., and Levelt, P. F.: Ozone mixing ratios inside tropical deep convective clouds from OMI satellite measurements, *Atmospheric Chemistry and Physics*, 9, 573–583, <https://doi.org/10.5194/acp-9-573-2009>, 2009.

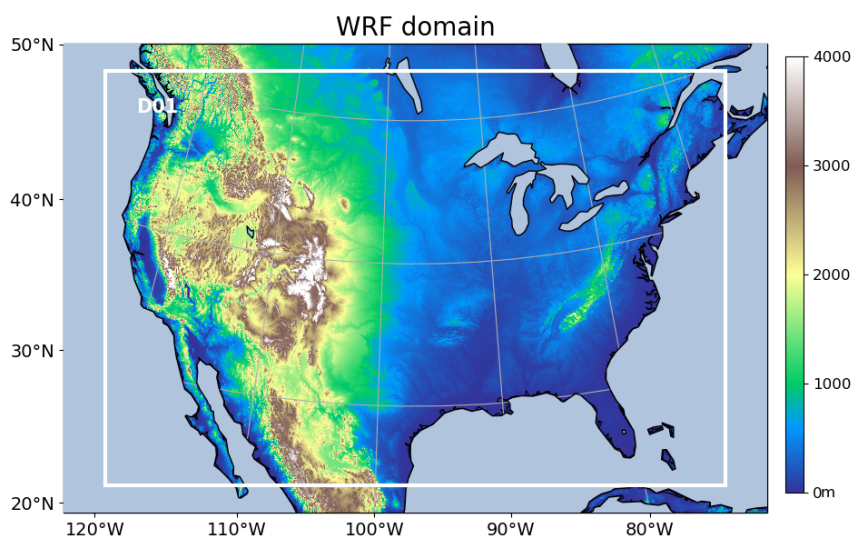


**Figure 1.** The 12-km resolution domain for WRF-Chem simulations.

**Table 1.** Definitions of the abbreviations for the criteria used in this study.

Abbreviations	Full form [source]
CRF	Cloud radiance fraction [OMI]
CP	Cloud optical pressure [OMI]
CF	Cloud fraction [WRF-Chem]
TL	Total lightning flashes [WRF-Chem]
ratio	modeled LNO <sub>2</sub> Vis / modeled NO <sub>2</sub> Vis [WRF-Chem]
crf <sub>α</sub> _entln	CRF ≥ α + entln flashes(strokes) ≥ 2400(8160) [ENTLN]
crf <sub>α</sub> _cf40_entln	CRF ≥ α + entln flashes(strokes) ≥ 2400(8160) + CF ≥ 40%
crf <sub>α</sub> _entln_tl1000	CRF ≥ α + entln flashes(strokes) ≥ 2400(8160) + TL ≥ 1000
crf <sub>α</sub> _cf40_entln_tl1000	CRF ≥ α + entln flashes(strokes) ≥ 2400(8160) + CF ≥ 40% + TL ≥ 1000
crf <sub>α</sub> _entln_tl1000_ratio50	CRF ≥ α + entln flashes(strokes) ≥ 2400(8160) + TL ≥ 1000 + ratio ≥ 50%
crf <sub>α</sub> _cf40_entln_tl1000_ratio50	CRF ≥ α + entln flashes(strokes) ≥ 2400(8160) + CF ≥ 40% + TL ≥ 1000 + ratio ≥ 50%

α has three options: 70%, 90% and 100%



**Table 2.** LNO<sub>x</sub> production under different conditions of CRF with coincident ENTLN data, TL ≥ 1000 and ratio ≥ 50%.

CRF (%)	ENTLN data type <sup>1</sup>	LNO <sub>x</sub> /flash or LNO <sub>x</sub> /stroke	R value	Intercept (10 <sup>6</sup> mol)	Days <sup>2</sup>
70	Flash	109.0 ± 15.3	0.84	0.23	85
90	Flash	114.8 ± 18.2	0.82	0.15	81
100	Flash	99.4 ± 15.3	0.84	0.10	71
70	Stroke	16.7 ± 2.6	0.79	0.58	96
90	Stroke	17.8 ± 2.9	0.78	0.29	93
100	Stroke	15.6 ± 3.1	0.75	0.16	82

<sup>1</sup>The threshold of ENTLN data is 2400 flashes box<sup>-1</sup> and 8160 strokes box<sup>-1</sup> during the period of 2.4 h before OMI overpass time. <sup>2</sup>The number of valid days with specific criteria in MJJA 2014.

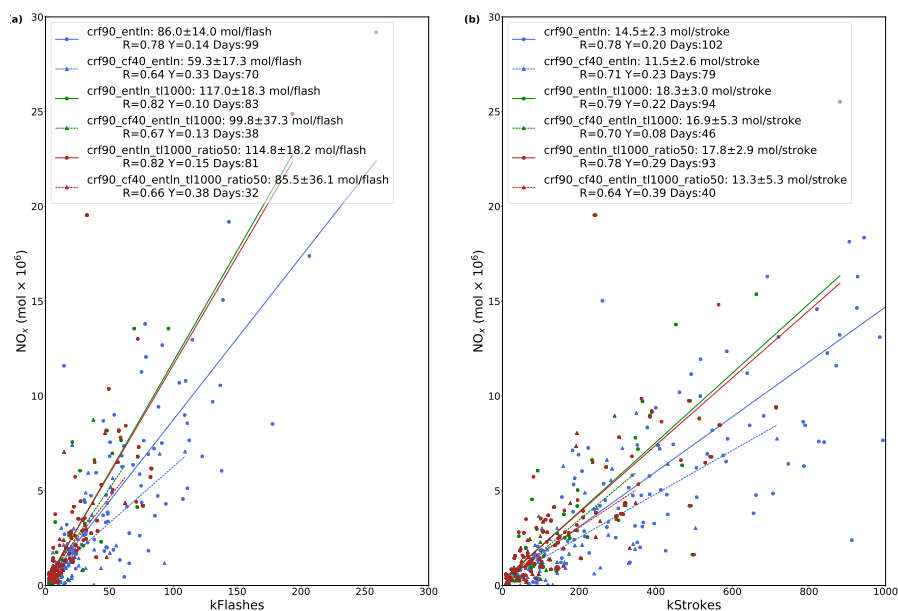


**Figure 2.** Linear regression of daily total LNO<sub>x</sub> summed over boxes with lightning 2.4 h prior to OMI overpass for MJJA 2014. (a) The comparison of LNO<sub>x</sub> production by six different combinations for CRF ≥ 90% with flash threshold of 2400 flashes. (b) Same as (a) except with a stroke threshold of 8160 strokes.

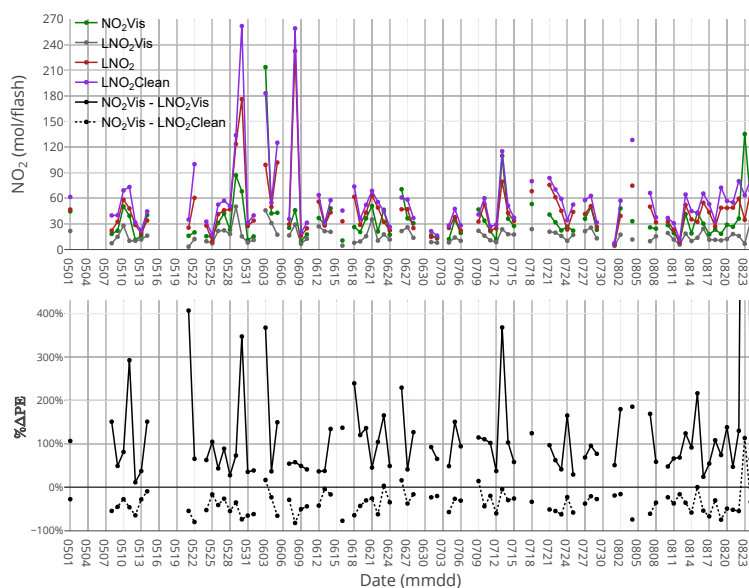


**Figure 3.** (top) Time series of  $\text{NO}_2\text{Vis}$ ,  $\text{LNO}_2\text{Vis}$ ,  $\text{LNO}_2$  and  $\text{LNO}_2\text{Clean}$  production per day over the CONUS for MJJA 2014 with  $\text{CRF} \geq 90\%$  and a flash threshold of 2400 flashes per 2.4 h. (bottom) Time series of the percent differences between  $\text{NO}_2\text{Vis}$  and  $\text{LNO}_2\text{Vis}$  and the percent differences between  $\text{NO}_2\text{Vis}$  and  $\text{LNO}_2\text{Clean}$  with  $\text{CRF} \geq 90\%$ . The value of black dot on August 23 (not shown) is 1958%.

**Table 3.** Uncertainties for the estimation of  $\text{LNO}_2/\text{flash}$ ,  $\text{LNO}_x/\text{flash}$ ,  $\text{LNO}_2/\text{stroke}$  and  $\text{LNO}_x/\text{stroke}$ .

Type	Perturbation	$\text{LNO}_2/\text{flash}^4$	$\text{LNO}_x/\text{flash}^4$	$\text{LNO}_2/\text{stroke}^4$	$\text{LNO}_x/\text{stroke}^4$
BEHR tropopause pressure <sup>1</sup>	NASA product tropopause	6	4	6	4
Cloud radiance fraction <sup>1</sup>	$\pm 5\%$	2	2	2	2
Surface pressure <sup>1</sup>	$\pm 1.5\%$	0	0	0	0
Surface reflectivity <sup>1</sup>	$\pm 17\%$	0	0	0	0
$\text{LNO}_2$ Profile <sup>1</sup>	$2 \times 500 \text{ mol NO flash}^{-1}$	13	26	13	26
Profile location <sup>1</sup>	Quasi-Monte Carlo	0	1	0	1
Lightning detection efficiency <sup>2</sup>	IC: $\pm 16\%$ , CG: $\pm 5\%$	15	15	15	15
$t_{\text{window}}^2$	2 – 4 hours	10	10	8	8
$\text{LNO}_x$ lifetime <sup>2</sup>	2 – 12 hours	24	24	24	24
$V_{\text{strat}}^3$	-	15	15	15	15
Systematic errors in slant column <sup>3</sup>	-	5	5	5	5
Net	-	37	43	36	43

<sup>1</sup>Laughner et al. (2019) <sup>2</sup>Lapierre et al. (2019) <sup>3</sup>Allen et al. (2019) <sup>4</sup>Uncertainty (%)



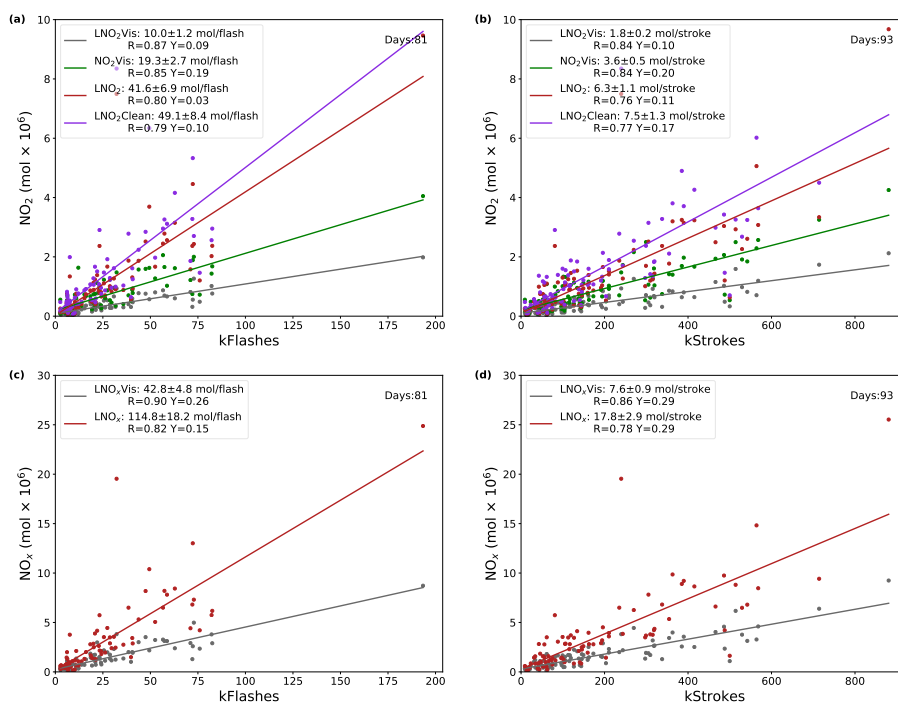


**Figure 4.** (a) Daily  $\text{NO}_2$  Vis,  $\text{LNO}_2$  Vis,  $\text{LNO}_2$  and  $\text{LNO}_2$  Clean versus ENTLN total flashes data. (b) Same as (a) but for strokes. (c) Daily  $\text{LNO}_x$  Vis and  $\text{LNO}_x$  versus total flashes. (d) Same as (c) but for strokes.

**Table A1.** Simple forms of abbreviations for AMFs.

Abbreviations	Numerator <sup>1</sup>	Denominator <sup>2</sup>
$\text{AMF}_{\text{LNO}_2}$	$S_{\text{NO}_2}$	$V_{\text{LNO}_2}$
$\text{AMF}_{\text{LNO}_2 \text{ Vis}}$	$S_{\text{NO}_2}$	$V_{\text{LNO}_2 \text{ Vis}}$
$\text{AMF}_{\text{LNO}_2 \text{ Clean}}$	$S_{\text{LNO}_2}$	$V_{\text{LNO}_2}$
$\text{AMF}_{\text{NO}_2 \text{ Vis}}$	$S_{\text{NO}_2}$	$V_{\text{NO}_2 \text{ Vis}}$
$\text{AMF}_{\text{LNO}_x}$	$S_{\text{NO}_2}$	$V_{\text{LNO}_x}$
$\text{AMF}_{\text{NO}_x \text{ Vis}}$	$S_{\text{NO}_2}$	$V_{\text{NO}_x \text{ Vis}}$

<sup>1</sup>The part of simulated VCD seen by OMI <sup>2</sup>The simulated VCD

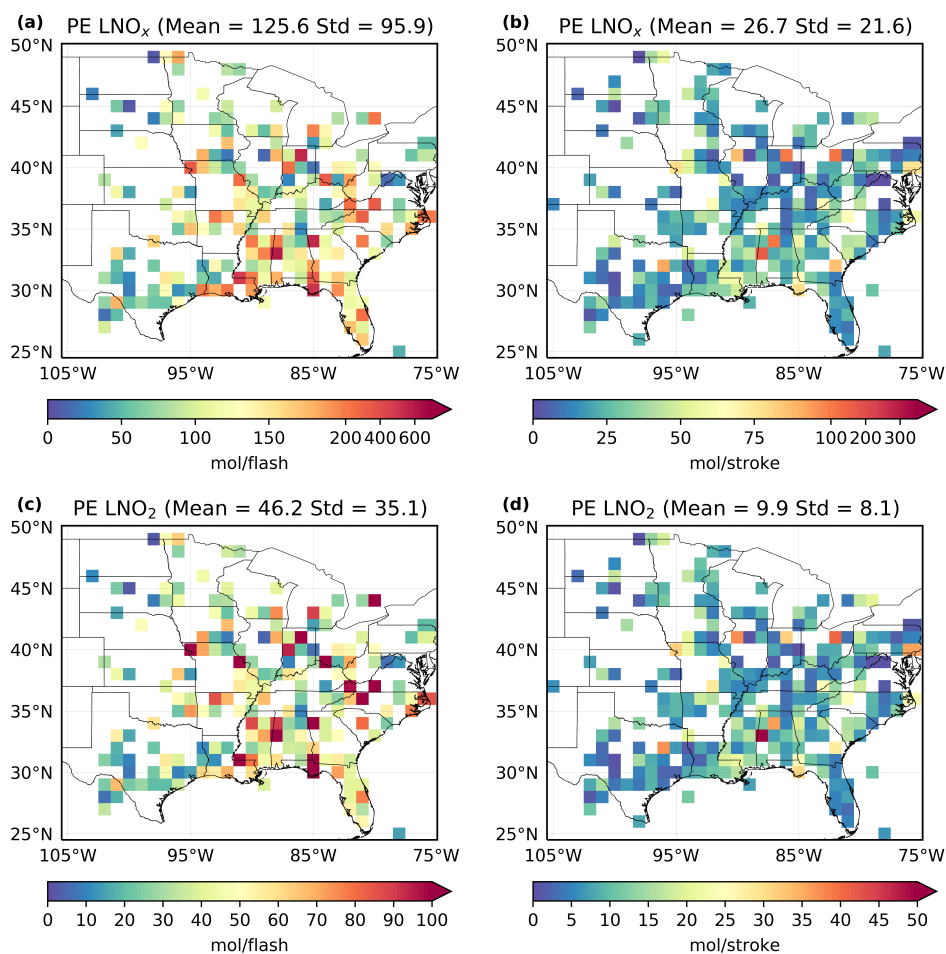


**Figure 5.** (a) and (c) Maps of  $1^\circ \times 1^\circ$  gridded values of mean LNO<sub>x</sub> and LNO<sub>2</sub> production per flash with CRF  $\geq 90\%$  for MJJA 2014. (b) and (d) Same as (a) and (c) except for strokes.

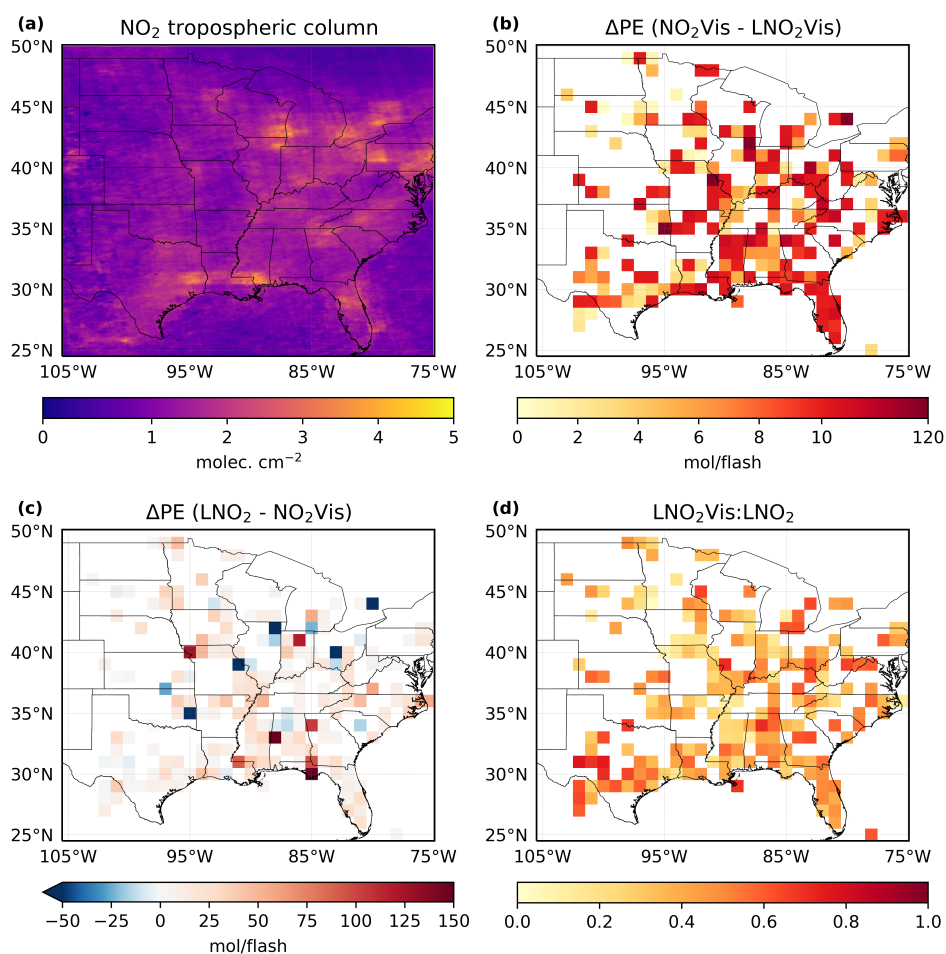


**Figure 6.** (a) Mean (MJJA 2014) NO<sub>2</sub> tropospheric column. (b) The differences of the estimated mean production efficiency between NO<sub>2</sub>Vis and LNO<sub>2</sub>Vis with CRF ≥ 90%. (c) The same differences as (b) but between LNO<sub>2</sub> and NO<sub>2</sub>Vis. (d) The ratio of LNO<sub>2</sub>Vis to LNO<sub>2</sub>.

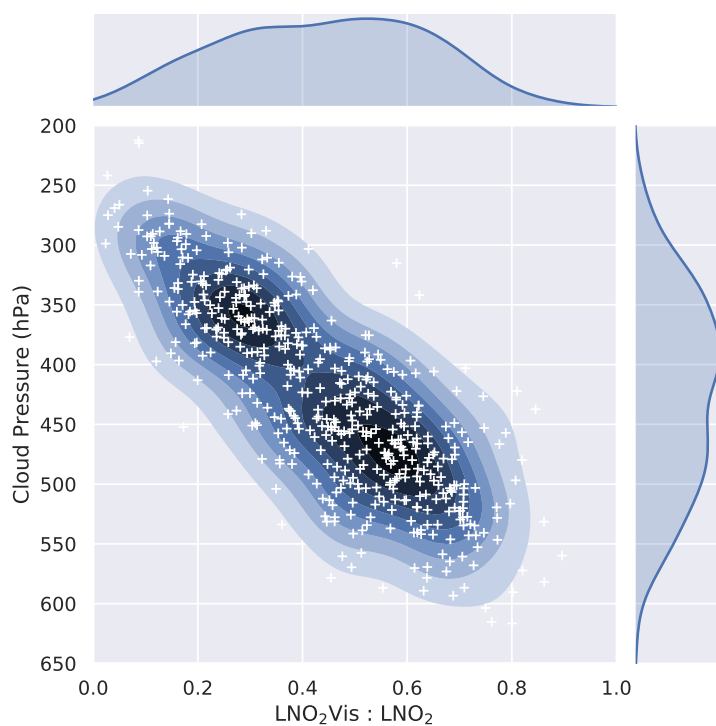


**Figure 7.** Scatter plots of the daily ratio of LNO<sub>2</sub>Vis to LNO<sub>2</sub> versus the daily cloud pressure measured by OMI with CRF  $\geq 90\%$  for MJJA 2014.

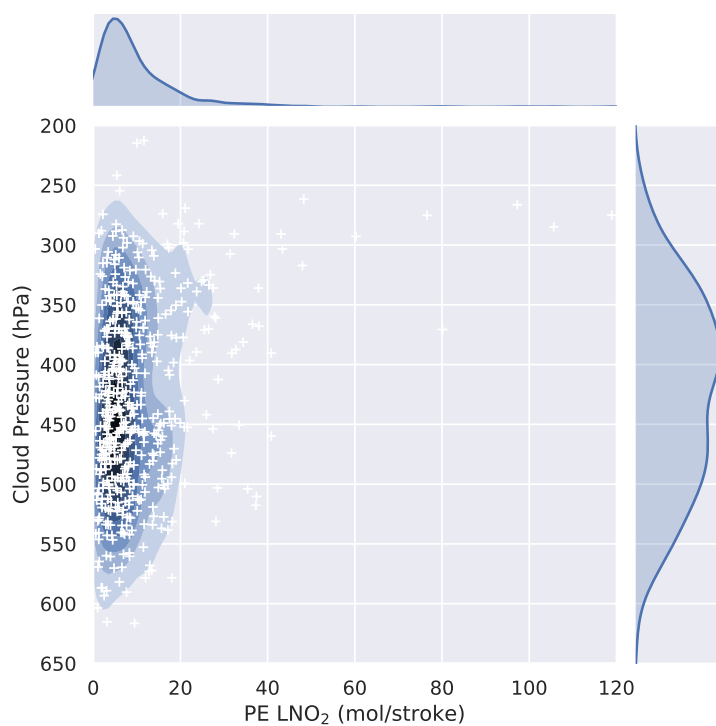


**Figure 8.** Scatter plots of the daily LNO<sub>2</sub> production efficiency versus the daily cloud pressure measured by OMI with CRF  $\geq 90\%$  for MJJA 2014.

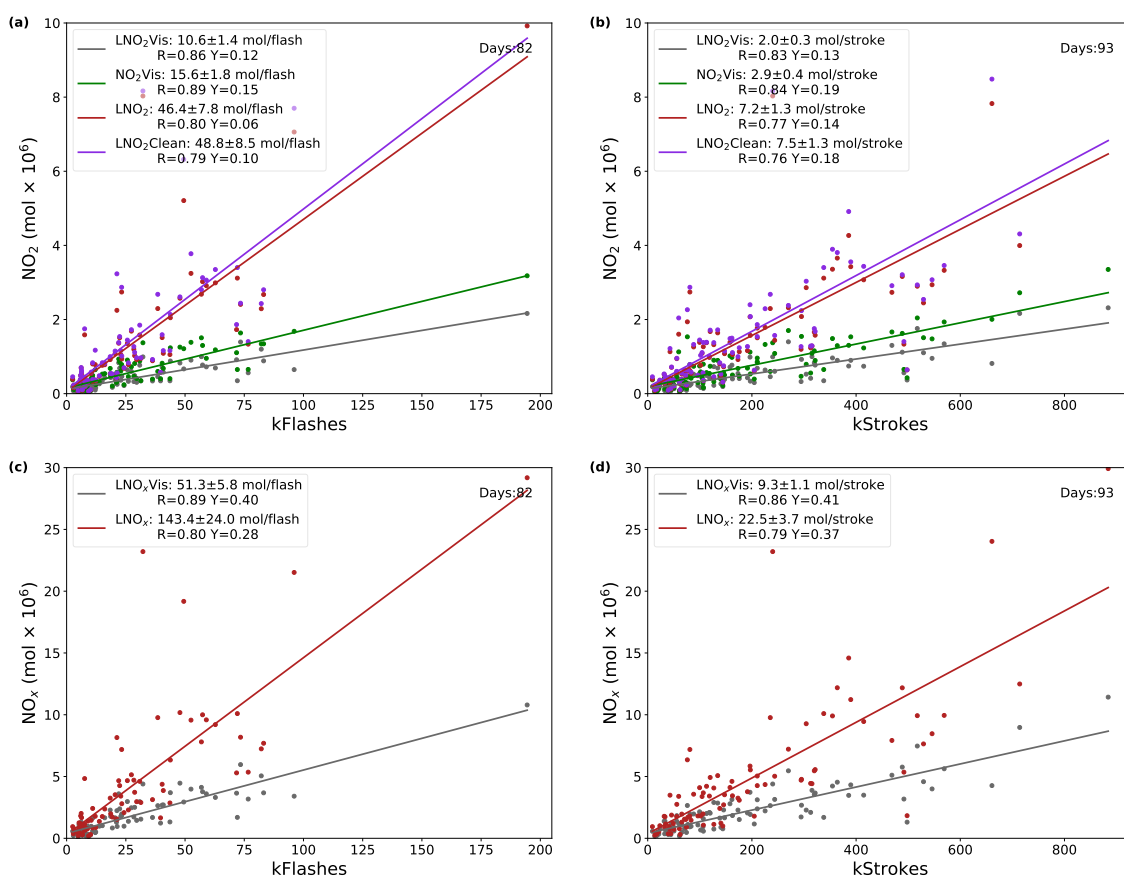
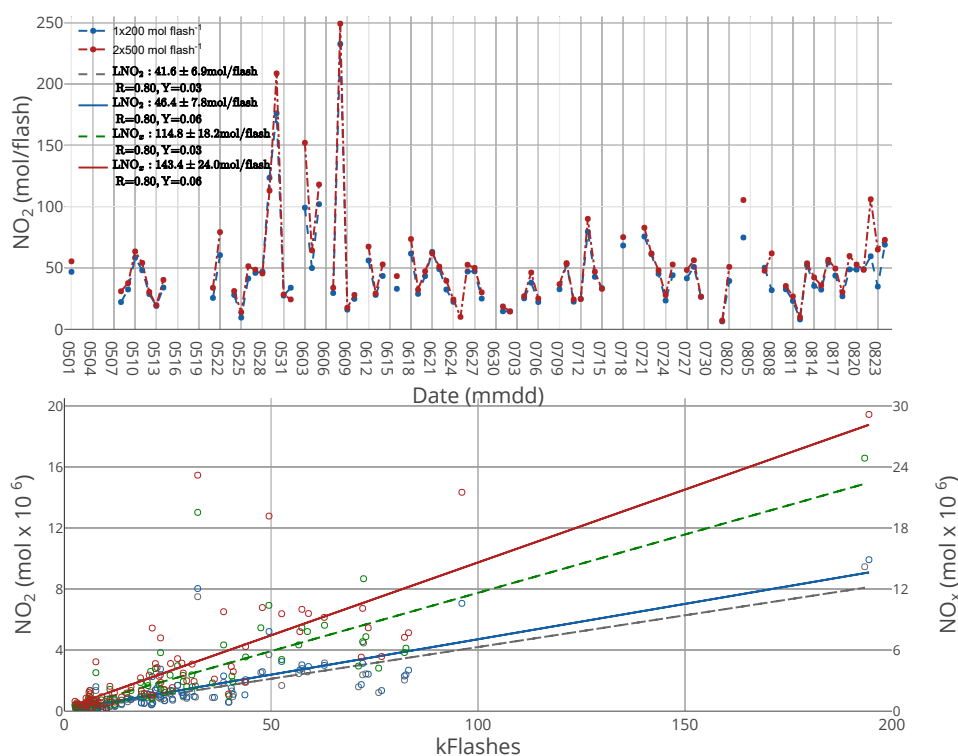
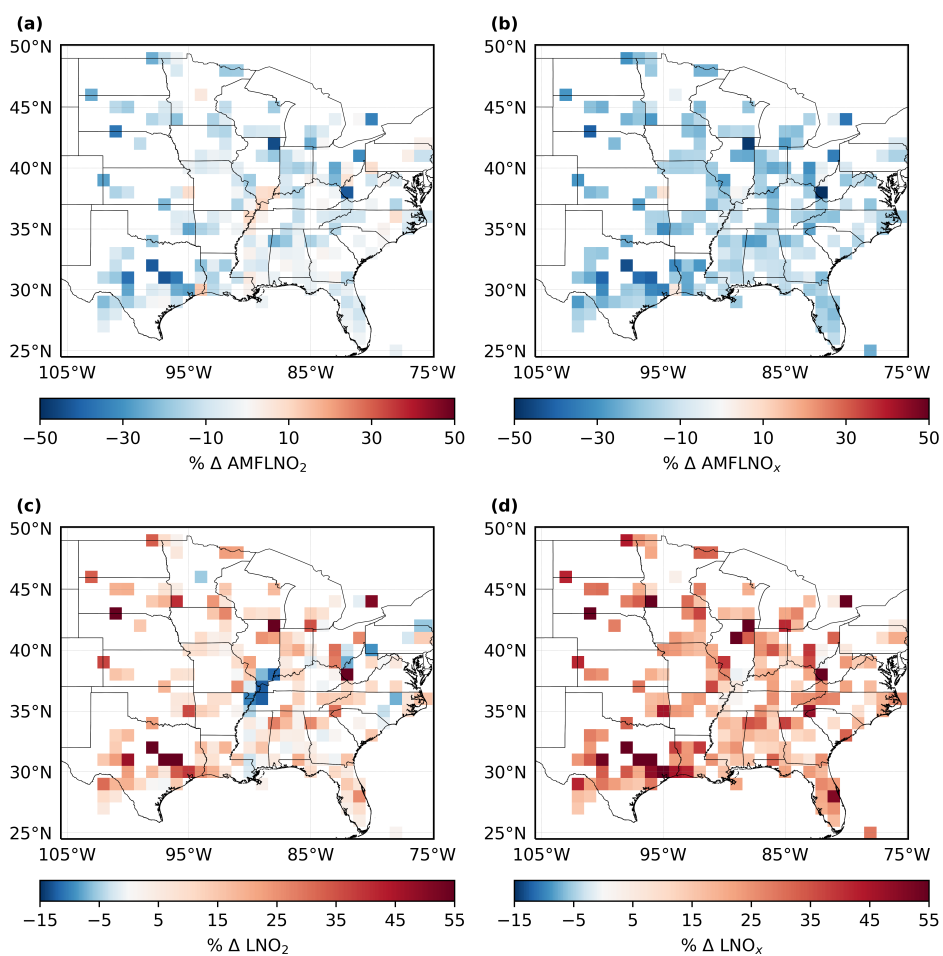


Figure 9. Same as Figure 4 except for 2 × 500 mol NO flash<sup>-1</sup> configuration.



**Figure 10.** (top) Time series of LNO<sub>2</sub> production per day over the CONUS for MJJA 2014 with CRF  $\geq 90\%$  and a flash threshold of 2400 flashes per 2.4 h. Blue lines mark the basic LNO configuration (200 mol NO flash<sup>-1</sup> and 1×base flashrate) while red lines mark 500 mol NO flash<sup>-1</sup> and 2×base flashrate. (bottom) Daily LNO<sub>2</sub> and LNO<sub>x</sub> versus ENTLN total flashes data. Dashed lines are based on basic LNO configuration while solid lines stand for the larger LNO configuration.



**Figure 11.** Average percent difference in (a)  $AMF_{LNO_2}$ , (b)  $AMF_{LNO_x}$ , (c)  $LNO_2$  and (d)  $LNO_x$  with  $CRF \geq 90\%$  over MJJA 2014. Difference between profiles are generated by  $2 \times 500 \text{ mol NO flash}^{-1}$  and  $1 \times 200 \text{ mol NO flash}^{-1}$ .



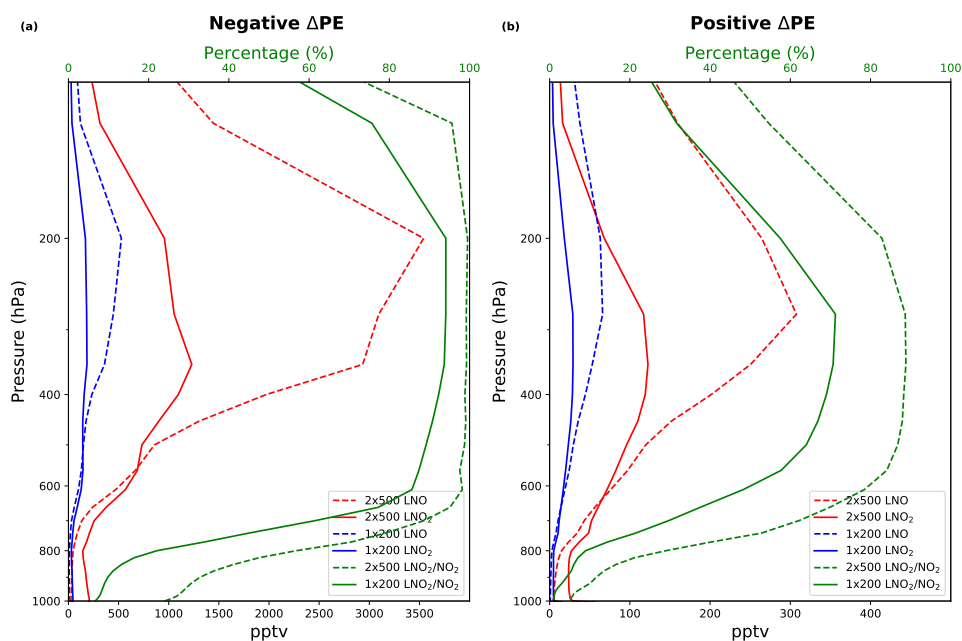


**Figure 12.** LNO and LNO<sub>2</sub> profiles with different LNO settings at (a) the region containing the minimal negative percent change in LNO<sub>2</sub> and (b) the region containing the largest positive percent change in LNO<sub>2</sub> when the LNO setting is changed from 1×200 mol NO flash<sup>-1</sup> to 2×500 mol NO flash<sup>-1</sup>, averaged over MJJA 2014. The profiles using 1×200 (2×500) mol NO flash<sup>-1</sup> are shown in blue (red) lines. Solid (dashed) green lines are the mean ratio of LNO<sub>2</sub> to NO<sub>2</sub> with 1×200 (2×500) mol NO flash<sup>-1</sup>.

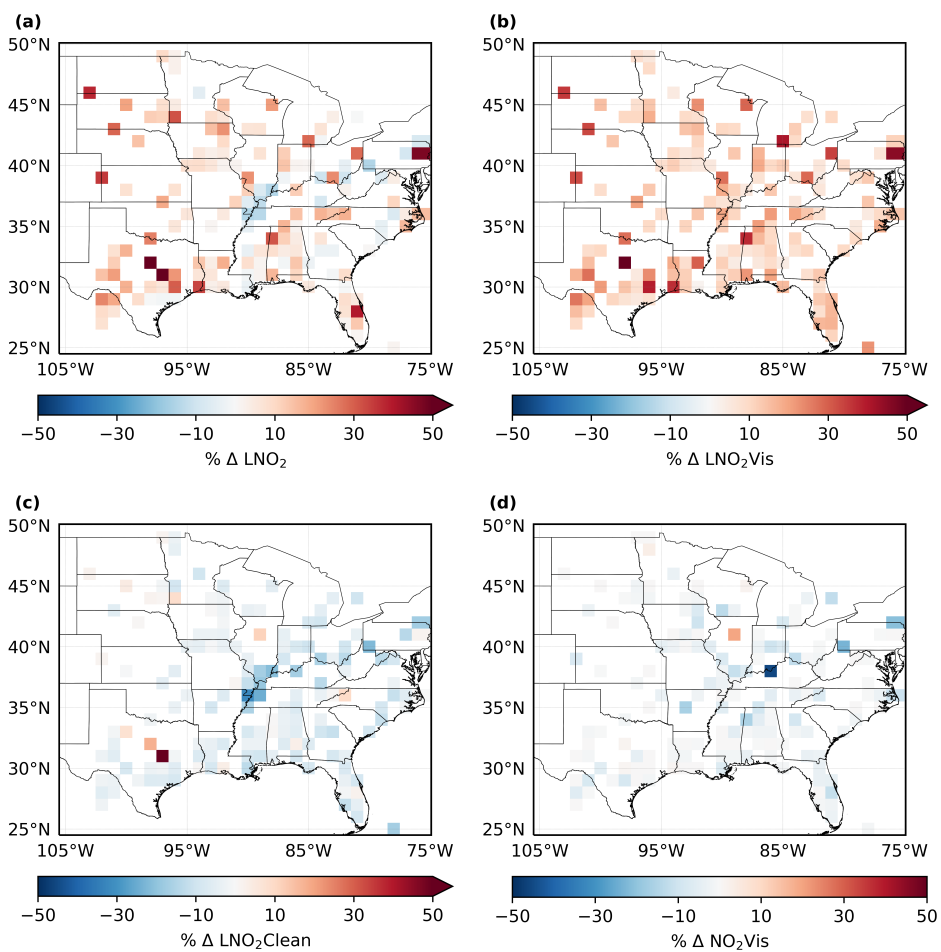


**Figure 13.** Average percent difference in (a) LNO<sub>2</sub>, (b) LNO<sub>2</sub>Vis, (c) LNO<sub>2</sub>Clean and (d)NO<sub>2</sub>Vis with CRF = 100% over MJJA 2014.